

**PHARMACOLOGICAL EVALUATION OF A SYNTHETIC COUMARIN
DERIVATIVE (4-FLOUROPHENYLACETAMIDE-ACETYL COUMARIN)
FOR ITS POTENTIAL ANTICANCER ACTIVITY IN NON-SMALL CELL
LUNG CANCER CELL LINE**

[Synopsis of PhD Thesis]

August, 2019

Ms. Shweta Umar



**DEPARTMENT OF ZOOLOGY, FACULTY OF SCIENCE
THE MAHARAJA SAYAJIRAO UNIVERSITY OF BARODA
VADODARA – 390 002, INDIA**

PHARMACOLOGICAL EVALUATION OF A SYNTHETIC COUMARIN DERIVATIVE (4-FLOUROPHENYLACETAMIDE-ACETYL COUMARIN) FOR ITS POTENTIAL ANTICANCER ACTIVITY IN NON-SMALL CELL LUNG CANCER CELL LINE

INTRODUCTION

Cancer is a complex disease characterized by rapidly proliferating transformed cells which has got enormous invasion as well as metastatic abilities¹. However, in spite of all the available modern medical intervention cancer therapy is still a major challenge. Further it has been reported that of all the cancers known worldwide, lung cancer, is the most frequently occurring in men, with a conspicuously high mortality rate. Moreover, out of the total incidents of lung cancer, non-small cell lung cancer (NSCLC) alone accounts for around 80-85%, of which adenocarcinoma is the most common type, claiming for 40% of the total occurrences². NSCLC is observed in many individuals irrespective of their dietary habits and the present medical advances like, surgery, chemotherapy, immunotherapy etc., are insufficient for its complete alleviation. On the contrary, the latter add to the complications by aggravating the side effects, and cause deleterious effects on surrounding healthy cells. Therefore, it is imperative to find a chemotherapeutic agent with least plausible side effects and higher specificity.

Coumarin is one such phytopharmacological agent which is widely known for its anti-cancer, anti-inflammatory³ and anti-coagulant properties⁴. These compounds and some of their derivatives are found naturally in tonka beans and cinnamon but they are present in a lesser amount, which makes the extraction process cumbersome. Therefore, chemical analogs of natural coumarin were synthesized. Some of these analogs, were marketed as fixatives, blood thinners and as drugs for the treatment of osteoporosis, but associated with severe side effects hence, not approved by FDA in United States⁵. One of the derivatives, which were used for treating lymphoedema in few European countries also got disapproved, due to its hepatotoxic effects⁶. Such drawbacks of the available coumarin derivatives, lead to more research, to chemically synthesize the ones with better selective and effective anticancer properties, along with least evasive effects. For the same, various pharmacophores are added to different positions of benzopyrone ring to enhance its biochemical and therapeutic properties.

In the current study, a string of derivatives were screened for their anticancer activity in

A549 cell line⁷ and found that 4-fluorophenylacetamide-acetyl coumarin (4-FPAC) showed significant cytotoxicity against A549 (NSCLC) human lung carcinoma cell line and exerts negligible side effect on a non-cancer cell line NIH3T3. Further, we investigated the effect of 4-FPAC on the cytotoxicity, cell cycle arrest and progression of metastasis in A549 cell line. Wherein, ETBr/AO, DAPI, Comet and LDH assay results revealed that 4-FPAC causing cytotoxicity via ROS induced p53 mediated mechanism, which involves both extrinsic and intrinsic pathways of apoptosis. DCFH-DA, Rhodamine123 and acridine orange staining confirmed that the ROS induced apoptosis involves both mitochondria and lysosome. Flow cytometric analysis revealed that derivative causes cell cycle arrest at G0/G1phase by p21 mediated downregulation of CDK2 and CDK4 cyclins. Aggregation, soft agar, clonogenic, scratch and parallel gene expression analysis collectively confirmed that the 4-FPAC minimizes the metastatic property of cell line via downregulating Snail, MMP-9 and IL-8. Additional studies confirmed the above finding and substantiates the role of PI3K/AKT in this.

In silico study was also done to elucidate the interaction through molecular docking between 4-FPAC and key target molecules i.e. p53. “Drug likeliness” reactivity and molecular electrostatic potential were also predicted, using ADME (Absorption, Distribution, Metabolism and Excretion), rule of five develop by Lipinski⁸ and Density functional theory (DFT) which includes HOMO-LUMO energies and molecular electrostatic potential (MESP). Due to virtue of its prolific anti-proliferative, anti-metastatic effect on lung cancer cells A549, along with the lesser side effects on the non-cancer ones with good ADME value and high reactivity 4-FPAC is competent to serve as a lead compound for future anticancer drug designing. The results based on the following objectives led to this conclusion.

OBJECTIVES

- To study the dose dependent cytotoxic effect of 4-FPAC on Non-small cell lung cancer cell line A549 and non-cancer cell line NIH3T3, 48 h post-treatment.
- To unearth the levels of reactive oxygen species and antioxidant enzymes in A549 cell line treated with 4-FPAC.
- To study the membrane potential loss in mitochondria and lysosome in 4-FPAC treated A549 cell line.
- To understand the extent of cytotoxicity through the flowing techniques - ETBr/AO, Morphology, LDH, Comet and DAPI. Parallely, cytostatic effect was followed using

Propidium Iodide based flowcytometry in A549 cell line.

- To assess the anti-metastasis property of 4-FPAC in A549 cell line using clonogenic inhibition, Soft agar, hanging drop and scratch assay.
- Molecular basis of cytotoxic and or cytostatic property of 4-FPAC was studied by analyzing the expression pattern of major genes involved in the said processes using techniques like qRT PCR and western blot.
- *In silico* prediction of derivative-target interactions, ADME, Molecular electrostatic potential and “drug likeliness” property was studied through molecular docking and DFT.

MATERIAL AND METHOD

Chemical and Reagent

The reagents were purchased from Sisco Research Laboratories (India), Gibco (USA) or Sigma-Aldrich (USA). After ascertaining the purity as described previously⁷, a stock solution of the coumarin derivative (4-flouorophenylacetamide-acetyl coumarin) was prepared in Dimethylformamide (DMF). Various dilutions of the derivative were prepared in phosphate buffer saline (PBS) wherein the final concentration of DMF was not more than 0.5% in any of the chosen aliquots.

Cell line procurement and maintenance

Human lung adenocarcinoma cell line A549 and mouse fibroblast cell line NIH3T, were purchased from National Centre for Cell Science (Pune, India). Cell lines were maintained in Dulbecco’s modified eagles medium (DMEM) supplemented with 2mM of l-glutamine and 10% fetal bovine serum with 1% antibiotic solution (Penicillin and streptomycin). The cells were maintained at 37°C with 5% CO₂ in a humidified CO₂ incubator (Thermo Fisher Scientific, USA).

MTT assay

The half minimal inhibitory concentration (IC₅₀ value) was evaluated using MTT assay. NIH3T3 cells were seeded in a 96-well plate (1×10³ cells/well) overnight in 100µl DMEM media supplemented with 10% FBS. 4-FPAC was added in 0.5, 1, 10, 25, 50, 75, 100 µM concentration and incubated for 48h. 20µl of MTT solution (5mg/ml prepared in PBS) was added and further the plate was incubated for 4h. Following incubation, supernatant was removed and the purple colored formazan crystals were dissolved in 100µl of acidified

Isopropanol. The absorbance (abs) was measured using microplate reader at 570 nm (Metertech Σ 960) and cell viability was calculated using following formula.

Cell viability (%) = (Average abs. of treated groups/Average abs. of control group) \times 100%.

Cell viability test

Cell viability test was performed by the dye exclusion test with 0.5% Trypan blue. 1×10^5 cells/well were seeded in 12 well plate and kept overnight for attachment. Next day cells were treated with 0.16 nM of 4-FPAC and incubated for 48h. DMF treated cells were taken as vehicle control whereas Triton X-100 treated ones served as positive control. Following incubation, cells were trypsinized and count was made using a hemocytometer⁹. Results were expressed as percentage of dead cells.

Cell cycle analysis

Effect of 4-FPAC on cell cycle distribution was analysed using BD FACS Area III flow cytometer. Cells were seeded at the density of 6×10^7 cells per T25 cm² flask. Cells were synchronized by serum free media for 24h followed by derivative treatment for 48h. Since, in all previous experiments there was no significant change observed between vehicle control and normal control, in the subsequent experiments only vehicle control (0.2% DMF) was used alongside the treatment group. Cells were trypsinized, and washed with PBS. Cell pellet was resuspended and fixed in ice cold 70% ethanol at -20°C for overnight. Next day, cells were centrifuged, collected and the cell pellet was washed twice with PBS, then incubated with RNAase (100 μ g/ml) and PI (50 μ g/ml) solution for 30 min at 37°C. 10,000 events per sub-population were analysed using BD FACSDIYA software (Becton Dickinson & CO., USA) as described by Chikara et al.⁹.

Cell morphology study

The cells from positive control, control and 4-FPAC treated group were seeded in a 12 well plate (2×10^5 cells/well). They were then incubated for 48h and observed under 20x magnification in Lawrence and Mayo (NIB 100) inverted microscope for their morphology.

Ethidium Bromide/ Acridine Orange staining

A549 cells were treated with 0.16 nM of 4-FPAC and incubated for 48h. Cells from both control and treated groups were then washed with PBS, trypsinized and stained with 10 μ l of EtBr/AO (100 μ g/ml). Ratio of stain to cell (1×10^3) was maintained as 1:25 μ l. Images were taken using DM2500 fluorescence microscope (Leica, Germany).

LDH assay

A549 cells were plated on 96 well plate (1×10^4 cells/well) for 24h in DMEM media without phenol red, followed by addition of various concentrations of 4-FPAC (0.5, 1, 10, 25, 50, 75, 100 nM). Subsequently, cells were incubated for 48h. Assay was performed according to the manufacturer's protocol (Pierce LDH Cytotoxicity Assay, Thermo Scientific, USA).

Comet assay

Effect of the 4-FPAC on apoptosis was observed using Comet assay. Derivative treatment was given as mentioned above in a 12 well plate. Cells were harvested in 10 μ l PBS and mixed with 10 μ l of 1% low melting point (LMP) agarose and was spread on the slide precoated with 1% normal melting point agarose. Three slides were prepared for each experiment and were kept for 20 min at 4°C, followed by coating of 0.75% LMP agarose for another 20 min at 4°C. After solidification of the components, slides were submerged in freshly prepared lysis buffer for 4h at 4°C. These were placed in electrophoretic chamber, filled with freshly prepared tank buffer (pH 8.3) and incubated for 30 min at 4°C. Electrophoresis was conducted at 200 mA / 22 V for 20 min at 4°C. Slides were thrice washed with neutralization buffer and allowed to dry for 5 min in absolute ethanol. Following this, cells were stained with Ethidium Bromide (20 μ g/ml). Slides were then observed under fluorescence microscope. At least 30 cells/slide were evaluated and components of comet assay were analysed using CaspLab software version 1.0.0. as suggested by Olive and Banáth¹⁰. DNA damage was expressed as % DNA in tail, % DNA in head, tail length, head length, total comet length, tail moment and olive tail moment.

Nuclear morphology study

Change in nuclear morphology and chromatin condensation was observed using DAPI (4, 6-diamidino-2-phenylindole). 1×10^3 cells were seeded on cover slips, which were placed in a six well plate and incubated at 37°C overnight for attachment. Following day, old media was replaced with the fresh one, containing 0.16 nM of 4-FPAC in case of treatment group and incubated for 48h. Further, the cells were washed with PBS and fixed with ice cold 70% ethanol, followed by permeabilization of the cells using 0.2% Triton X-100. Cells were then, stained with 10 μ g/ml DAPI solution for 15 min at room temperature¹¹ and images were taken using fluorescence microscope.

Analysis of reactive oxygen species

Dichlorodihydrofluorescein diacetate (DCFH-DA) staining was used for the determination of intracellular ROS levels. Cells were seeded on 6 well plate (5×10^5 cells/well), treated with IC_{50} concentration of 4-FPAC for 48h then harvested by trypsinization following which, the pellet was washed with PBS and stained with $25 \mu\text{M}$ of DCFH-DA dye. H_2O_2 was used as positive control. Stained cells were incubated for 40 min. Image was captured using Leica DM2500 fluorescence microscope.

For total ROS detection in A549 cell, 5×10^5 cells/well were seeded in 6 well plate overnight. Next day, cells were treated with IC_{50} concentration of 4-FPAC and incubated for 48h. Following incubation, cells were harvested by trypsinization, washed with PBS and again re-suspended in $100 \mu\text{l}$ PBS containing $10 \mu\text{M}$ DCFH-DA and incubated for 40 min. Equal number of cells in $100 \mu\text{l}$ PBS were used for each fluorimetry detection. Tubes were read at 480 nm in Qubit® 2.0 Fluorometer (Invitrogen, USA) and graph was plotted against change in ROS level¹².

Sample preparation for biochemical estimations

70-80% confluent cells were treated with IC_{50} value of 4-FPAC, after 48h of incubation, they were trypsinized and the pellet was washed with pre-chilled PBS. Pellet was resuspended in extraction buffer (0.1% Triton X-100 and 0.6% sulfosalicylic acid in KPE) homogenized, and sonicated in ice for 2-3 min. Lysate was centrifuged at 3000 g for 4 min at 4°C and the supernatant was collected in pre-chilled tube for detection of enzymatic assay.

Glutathione peroxidase (GPx)

Reaction mixture contained $200 \mu\text{l}$ Phosphate buffer (0.4 M pH 7), $100 \mu\text{l}$ glutathione (2mM), $200 \mu\text{l}$ NaN_3 (10mM), $200 \mu\text{l}$ H_2O_2 (10mM) and $100 \mu\text{l}$ water, $40 \mu\text{l}$ of supernatant. It is then incubated for 5 min at RT followed by addition of $200 \mu\text{l}$ meta phosphoric acid (30mM). It was further kept in ice for 10 min followed by centrifugation at 2000 rpm for 10 min. Of the supernatant collected, $60 \mu\text{l}$ was incubated with $60 \mu\text{l}$ of Na_2HPO_4 (0.4 M) and $3 \mu\text{l}$ DTNB following which, reading was taken at 412nm in microplate reader. The blank contained all the reagents except the supernatant¹³. The activity of GPx was expressed as nM of glutathione oxidized per minute per milligram protein.

Superoxide dismutase (SOD)

SOD activity of supernatant was assayed using a method based on its capacity to inhibit pyrogallol auto-oxidation, under standard assay condition¹⁴. $50 \mu\text{l}$ potassium phosphate

buffer (0.2 M, pH - 8) and 5 μ l pyrogallol (25 mg pyrogallol in 1ml of 0.5N HCl) was added in 3 μ l of supernatant, reading was taken at 420 nm in microplate reader. Blank contained all the reagents except the supernatant.

Unit of SOD/ml of assay mixture was calculated = $(A-B/A \times 50) \times 100$

Where A = abs of substrate blank and B = abs of substrate test.

Catalase (CAT)

Supernatant was mixed with 50 μ l of H₂O₂ (0.2 M) and 80 μ l PBS (0.01M pH7), incubated for 1 min at RT then 80 μ l dichromic acetic acid reagent (5% K₂Cr₂O₇ in 1:4 glacial acetic acid) was added and boiled for 10 min, allowed to cool down, while absorbance was taken at 570 nm in microplate reader. Blank contained all the reagent except supernatant¹⁵.

Catalase activity = $[(\text{Sample OD} \times \text{Volume of assay}) / \text{Aliquot} \times \text{CF}]$

Where CF = 0.0041

Result expressed as μ mole of H₂O₂ decomposed / μ g protein.

Detection of mitochondrial membrane potential

For the detection of mitochondrial membrane potential Rhodamine 123, a fluorescent dye which binds only to metabolically active mitochondria was used. Cells were seeded on coverslip in 6 well plate and incubated overnight for attachment, next day, old media was replaced with fresh medium containing IC₅₀ concentration of 4-FPAC and incubated for 48h, followed by washed with PBS. Cells were fixed with ice cold 70% ethanol and further incubated for 30 min at 37°C with 5 μ g/ml Rhodamine 123. Cells were then washed with PBS and photographed using Leica DM2500 fluorescence microscope.

Detection of lysosomal membrane permeabilization

Acridine orange is a lysosomotropic weak basic dye which stains the lysosome red when there is a drop of proton gradient due to deterioration of the lysosomal membrane integrity. In case of intact lysosomes protonated AO exhibits red fluorescence and translocation of lysosomal content to the cytosol during lysosomal stress results in deprotonation of AO with green fluorescence. Cells were plated on coverslip and treated as previous with IC₅₀ concentration of 4-FPAC, after 48h of which, these same cells were treated with 5 μ g/ml AO solution and incubated for 15 min. Images were captured using Leica DM2500 fluorescent microscope¹⁶.

Clonogenic inhibition assay

For determining colony formation ability of the cell line under the influence of 4-FPAC, clonogenic inhibition assay was performed. Cells were trypsinized at log phase and 1×10^3 cells/ml were plated on 35mm plate, followed by treatment with 0.16 nM of derivative. After 48h, old media was replaced with new and the cells were further incubated for 10 days. Thereafter, cells were fixed and stained with 0.1% crystal violet solution. Number of colony was counted using Image J software (NIH). The surviving fraction was calculated as the ratio of the number of colonies formed after treatment to the product of the number of cells plated and the plating efficiency¹⁷.

Soft agar assay

Anchorage independent growth is a decisive property of cancer metastasis and growth. This adhesion independent growth, under the influence of 4-FPAC was evaluated by using soft agar assay. 35mm disc was coated with 0.8% agarose in FBS free media, once solidified, it was overlaid with 0.4% agarose with cell and left to solidify. Media with IC₅₀ concentration of 4-FPAC was added for 48h. It was then replaced with fresh one and incubated for 10 days. On eleventh day, cells were stained with 0.01% crystal violet solution and photographed under microscope. Number and size (pixels) of the colony was counted using Image J software (NIH)¹⁸.

Wound healing assay

Cancer cell migration was analyzed using wound healing assay. Cells were seeded on 6 well plate with the density of 2×10^5 cells/well in media supplemented with 10% FBS. Cells were incubated overnight to adhere and form monolayer. Once the monolayer reached 90% confluence, it was scratched with the help of 20 μ l pipette tip, then washed with PBS to remove the detached cells completely. Thereafter, the old medium was replaced with fresh one containing IC₅₀ of 4-FPAC. Image was taken using inverted microscope at 0h, followed by incubation for 48h, in 1% serum medium and was photographed using Lawrence and Mayo inverted microscope and evaluated using Image J software (NIH). Wound area covering was compared using Student's t test at 95% significance, wherein, experiment was done in triplicates with 3 scratches each, for both, control and treated¹⁹.

Hanging drop aggregation assay

Aggregation property of the cell line was analyzed using hanging drop method. Cells were

harvested, centrifuged and counted. 2×10^6 cells/ml were re-suspended from stock in media containing IC_{50} of 4-FPAC and for control, same number of cells were incubated in media without derivative. $30 \mu\text{l}$ of cells suspended media was placed as droplet on the inner side of the 60mm petri dish lid and 20 droplets per lid were placed and incubated for 48h. 10 ml of media was poured in the disc to avoid evaporation. Image was taken at 0h and 48h for both control and treated. Total area covered by aggregate was analyzed using Image J software (NIH) and mean area of aggregate was expressed in pixels.

Gelatin zymography

1×10^6 cells/well were seeded in a 6 well plate incubated overnight, followed by treatment with IC_{50} concentration of 4-FPAC. After 48h, media was removed and cells were washed with cold PBS. Thereafter, the cells were homogenized in lysis buffer (Tris-Cl 10mM pH 8, NaCl 150mM, $CaCl_2$ 10mM and 1% Triton X-100), centrifuged and the supernatant was taken and concentration of protein was estimated using Bradford. $30 \mu\text{g}$ of protein was used for SDS-polyacrylamide gel electrophoresis, containing 2.5% gelatin in resolving gel. Electrophoresis was done at 100V. Gel was washed twice with Triton wash buffer followed by two incubation buffer washes of 15 min each. It was then left for further incubation overnight at 37°C , followed by staining with 0.25% Coomassie brilliant blue for 4h and de-staining till clear band were seen on blue background.

Western blot analysis

Protein from treated and control cells was harvested as mentioned for zymography. $40 \mu\text{g}$ of protein was used for the SDS-PAGE electrophoresis. The separated sample was transferred onto PVDF membrane at 100 mA for 20 min. After that, blocking was done with TBS containing 0.1% Triton X-100 and 5% skimmed milk for 1h. Thereafter, membrane was incubated with primary antibodies which were, monoclonal anti-MMP-9 IgG goat $0.1 \mu\text{g/ml}$ (Sigma Aldrich USA), anti-IL-1 β IgG rabbit $0.1 \mu\text{g/ml}$ (Sigma Aldrich USA), anti- β -catenin IgG mouse $0.1 \mu\text{g/ml}$ (Santacruz biotechnology USA), anti-PCNA IgG rabbit $0.1 \mu\text{g/ml}$ (Sigma Aldrich USA), anti-cleaved Caspase 3 IgG rabbit $0.1 \mu\text{g/ml}$ (Sigma Aldrich USA), anti-VEGF- α IgG goat $0.5 \mu\text{g/ml}$ (DSHB IOWA), anti-AKT IgG rabbit $0.1 \mu\text{g/ml}$ (Sigma Aldrich USA), anti-TNF- α IgG mouse $0.1 \mu\text{g/ml}$ (Sigma Aldrich USA), anti-iNOS IgG rabbit $0.1 \mu\text{g/ml}$ (Sigma Aldrich USA), anti-IL-6 IgG mouse $0.5 \mu\text{g/ml}$ (DSHB IOWA), anti-E-cadherin IgG mouse $0.5 \mu\text{g/ml}$ (DSHB IOWA), anti-N-cadherin IgG mouse $0.5 \mu\text{g/ml}$ (DSHB IOWA), anti-vimentin IgG mouse $0.5 \mu\text{g/ml}$ (DSHB IOWA), anti-PI3K IgM

mouse 0.5 µg/ml (DSHB IOWA), anti-Grb7 IgG mouse 0.5 µg/ml (DSHB IOWA) and anti-β-actin IgG mouse 0.1 µg/ml (Santacruz biotechnology USA)) at 4°C for 16h. Followed by three washes with wash buffer (50mM Tris HCl of pH 7.6, 150mM NaCl and 0.1% Tween 20) and each wash last for 15 min. Then incubated with corresponding biotinylated secondary antibody (0.5 µg/ml) for 45 min at room temperature, followed by three washes. After that, membrane was incubated with ALP conjugated streptavidin (0.5 µg/ml) for 45 min, washed thrice as mentioned earlier. Bands were developed upon addition of BCIP-NBT substrate (Sigma-Aldrich, St Louise, MO).

Quantitative real time PCR

Total RNA was isolated from using TRIzol reagent and purity of RNA was checked by the ratio of A₂₆₀ nm by A₂₆₀ nm. 1µg of DNAase free RNA was reverse transcribed into cDNA using cDNA Synthesis Kit (Applied Biosystems, USA). Real time RT PCR (LightCycler 96 Roche Diagnostics, Switzerland) was performed using primers for genes viz. *p53*, *p21*, *BCL-2*, *MDM2*, *survivin*, *BID*, *BAX*, *BAD*, *AIF*, *PARP1*, *β-catenin*, *cathepsin B*, *calpain 2*, *PCNA*, *caspase 3,9,7, 8*, *cytochrome c*, *TRADD*, *FADD*, *cyclin D1*, *CDK2*, *cyclin E*, *CDK4*, *HIF-1α*, *IL-8*, *TGF-β*, *IL-10*, *iNOS*, *MMP9*, *MMP2*, *TIMP2*, *TIMP4*, *E-cadherin*, *N-cadherin*, *vimentin*, *snail1*, *snail2*, *ZEB1*, *claudin 3(CLDN3)*, *claudin 4(CLDN4)*, *VEGF-α*, *VEGF-R/KDR* and *AKT*. 18srRNA was used as endogenous control for normalization of data. Gel electrophoresis and melt curve analysis were used for confirmation of specific product formation. Fold change was calculated using Livak method ($2^{-\Delta\Delta Cq}$)²⁰.

Computational methods

***In silico* study**

All computational studies were carried out using Workstations from Supermicro with configurations of Intel® core™ I7p-2600 CPU @ 3.40 GHZ, Operating System CentOS 6.3, Desktop from Lenovo with configurations of Intel ® Core™ 2 Duo CPU E7300@2.66GHZ.

Ligand preparation

The compound 4-FPAC was generated using chem Draw ultra 2012. the sketched ligand structure was prepared using LigPrep, an application of Maestro (LigPrep, version 3.4, Schrödinger, LLC, New York, NY, 2015). Different ionization states were generated at neutral pH using Epik (version 3.2 Schrödinger, LLC, New York, NY, 2015), geometry and charges were optimized using OPLS2005 force field. Ligprep is a utility in Schrödinger

software suit that ensures optimization of ligand geometry, minimizes the energy of 3D structure and give best tautomeric and steric isomer with minimized energy for docking.

Protein preparation

X-ray crystallographic structure of target proteins i.e. p53 was retrieved from Protein Data Bank (PDB) viz. PDB ID. 5LGY and prepared for docking using protein preparation wizard (Schrödinger Suite 2015 Protein Preparation Wizard Schrödinger, LLC, New York, NY, 2014) in Maestro (Maestro, version 10.2, Schrödinger, LLC, New York, NY, 2015). Protein preparation is a multistep process in which wizard adds missing bond, assigns correct bond order and charges, removes any crystallographic water whereas, hydrogens remain unstrained and geometry of the input protein remains unaltered; instead it checks for any problems in the protein structure and corrects them. This optimized structure was further energy minimized, using the OPLS2005.

Active site prediction

The active site residues of PDB ID. 5LGY was obtained by the literature²¹.

Induced fit Docking

Ligand and protein were docked with Schrödinger's induced fit protocol by using Glide software to exhaustively consider possible binding modes and the associated conformational changes within receptor active sites. This unique procedure allows to quickly predict active site geometries with minimal expense. Maestro, the graphical user interface for the Schrödinger software, allows easy execution of induced fit simulations and also aids in result interpretation. Once the receptor grid was generated, the ligand 4-FPAC was docked to the receptor using Glide (version 6.7) docking protocol with default parameters under the-Extra precision (XP) model²².

Electronic properties

DFT analysis (*HOMO- LUMO and MESP*)

Conformations obtained from the Docking protocol generated using IFD was used as input for density functional theory (DFT) calculations. All DFT calculations were carried out using Jaguar version 9.8 Schrödinger, installed on Intel core i7-2600 CPU @ 3.40GHZ. Complete geometry optimization was carried out using hybrid density functional theory with Becke's three parameter exchange potential and the Lee-Yang-Parr correlation functional

(B3LYP), using basis set 631G**++ level. To simulate physiological conditions, energy calculations were performed in aqueous environment using the Poisson-Boltzmann solver. The molecular electrostatic properties including MESP maps (MESP isoenergy contours generated at -30.0kcal/mol), HOMO and LUMO were computed. Jaguar (Schrödinger); an *ab initio* quantum chemical program specializes in fast electronic structure predictions of molecules. Calculating the electronic structure of molecules may play an important role in understanding of the structure, activity, and dynamics of a molecule which presents a computational approach to drug designing²³.

ADME Prediction for 4-FPAC

4-FPAC was evaluated for its drug-likeness through ADME properties using QikProp module inbuilt in Schrödinger software suite. This software helps predict physically significant descriptors and pharmaceutically relevant properties of molecules. Candidate molecules are assessed based on the biological properties such as the predicted octanol/water partition coefficient (QPlogPo/w), octanol/gas partition coefficient (QPlogPoct), water/gas partition coefficient (QPlogPw), human oral absorption in intestine (QP%), brain/blood partition coefficient (QPlogBB), apparent Caco-2 cell permeability in nm/sec (QPPCaco) and apparent MDCK cell permeability in nm/sec (QPPMDCK). Evaluation of drug-likeness of a compounds was based on the Lipinski's rule of 5; (number of violations of Lipinski's rule of five) essential for rational drug design.

Statistical analysis

All values are reported as mean \pm SD. Experiments were performed in triplicates. Statistical analysis was performed using GraphPad Prism 5 software. The difference between groups was analyzed using one-way ANOVA or Student's t test. Level of significance was kept at 95%.

RESULTS

4-FPAC induces cytotoxicity in A549 cell line.

The metabolic viability of 4-FPAC on non-cancer cell line (NIH3T3) was evaluated using MTT assay and found to be $79.58 \pm 10.24 \mu\text{M}$ (Figure1B). Since, 4-FPAC could effectively curb the viability in A549 cell line at a very low dose (0.16 nM)⁷, compare to NIH3T3, it is presumed that at this concentration 4-FPAC will not cause any deleterious effect to neighboring non-cancer cells.

In trypan blue exclusion assay, treatment with IC₅₀ concentration of 4-FPAC showed 28% death in A549 cell line, whereas, no significant difference in cell death was observed between control and vehicle control groups (Figure 1C). However, the reported metabolic viability in MTT assay was found to be 50% at this concentration⁷, which highlights the quiescent stage of the cells, wherein the cells are not dead, but elicit arrested growth. Therefore, it could be deduced that 4-FPAC was not only showing cytotoxic but also cytostatic property.

4-FPAC causes cell cycle arrest at G0/G1 phase.

Effect of 4-FPAC on cell cycle was analysed using Propidium iodide staining through flow-cytometry and it was observed from the histogram that 46.8% of cells were in G0/G1 phase and only 40.9% of cells were in sub G0/G1 phase when compared with control cell where most of the cells were equally distributed which showed that 4-FPAC arrest the cells in G0/G1 phase of cell cycle (Figure 2).

The cell cycle genes including check-point genes viz., *cyclin D*, *CDK2*, *CDK4*, *cyclinE*, *PCNA*, *p21*, *p53* were analysed using qRT PCR and at transcript level a significant increase was observed in the expression of *p53*, *p21* and *PCNA*. However, the expression of *CDK4*, *cyclin D (CCND)*, *CDK2* and *cyclin E (CCNE)* were found significantly decreased (Figure 3A). Nonetheless, the western blot analysis of PCNA, a proliferation marker, revealed that there was no significant change at protein level (Figure 3B).

4-FPAC induces apoptosis in A549 cell line

Morphology of A549 cells at IC₅₀ concentration was observed after 48h of 4-FPAC treatment. Apoptotic features like granulation, rounding of cell and detachment from substratum were frequently observed in the 4-FPAC treated group (Figure 3C). No visible change in morphology was observed in DMF treated cells (Figure 3B), which indicate that the vehicle caused no significant alteration in cell morphology. However, triton X-100, which served as positive control, treatment resulted in greater loss of attachment and more rounding of cell (Figure 3D).

Subsequently, cell death and its mechanism were analysed by dual staining method using EtBr/AO dye which gives green colour if cells are alive, orange/yellow if cells are in early

or late apoptosis and red, if cells are under necrosis. In control (Figure 3E) and vehicle control groups (Figure 3F) most of the cells were green when compared with 4-FPAC treated group (Figure 3G) where maximum cells were in early or late apoptotic stage as exemplified by the yellow/orange colour. However, all cells in the positive control were red (Figure 3H). The current result indicates that 4-FPAC treated cells were undergoing apoptotic type of cell death.

The analysis of LDH released by the 4-FPAC treated cells revealed that the derivative induces cytotoxicity in a dose dependent manner and at IC₅₀ concentration no significant release of LDH was noticed hence consolidating the fact that at this concentration 4-FPAC induced cell death by apoptosis (Figure 3I)

4-FPAC induces genotoxicity in A549 cell line

Genotoxic effect of 4-FPAC was analyzed by comet assay, DNA damage was represented in the form of comet tail length. The result revealed that unlike control (Figure 5A) and vehicle control groups (Figure 5B), 4-FPAC treated cells (Figure 5C) showed ample signs of DNA damage which were quite comparable to that of positive control (Figure 5D). The percentage head DNA, percentage tail DNA, tail moment and olive tail moment in A549 is presented in Table 1.

The morphological evidence of apoptosis like chromatin condensation, nuclear fragmentation and margination of nucleus were further confirmed by DAPI staining. No visible sign of chromatin condensation and margination was observed in control (Figure 6A) and vehicle control group (Figure 6B) whereas in 4-FPAC treated cells, chromatin condensation could be seen frequently (Figure 6C).

4-FPAC treatment hampers the balance between ROS and antioxidant enzymes

ROS plays a very critical role in cancer cell proliferation as well as in cellular toxicity. Many chemotherapeutic agents induce apoptosis in cancer cells by augmenting the intracellular ROS concentration beyond the threshold level²⁴. The antioxidant enzyme system, which regulates ROS concentration and maintains the cellular redox equilibrium, includes Superoxide dismutase, Catalase and Glutathione peroxidase. These antioxidant enzymes act by metabolizing the free radicals which might damage the cell²⁵. Herein the ROS level was measured using fluorimeter (Figure 7D). Further, the morphology of the cell was analysed

to ascertain that the ROS generation was not due to cellular damage. There was an increase in fluorescence of treated cell line (Figure 7B) as compared to the control one (Figure 7A) which revealed a significant increase in intracellular ROS level. 4-FPAC might be exerting its cytotoxic effect on A549 cell via increased intracellular ROS concentration as it plays a major role in induction of apoptosis.

The activities of Superoxide dismutase, Catalase and Glutathione peroxidase were also evaluated in the treated as well as control cells at 24h and 48h. The analysis of the result revealed that at 24h the activities of the studied antioxidant enzymes in the 4-FPAC treated cells remained at the basal level except for that of GPx (Figure 8B) which registered a significant increase. However, at 48h a significant decrease in the activities of catalase (Figure 8A) and glutathione peroxidase were observed but no change in superoxide dismutase (Figure 8C) in the treated cells compared to that of control.

4-FPAC treatment disrupts membrane potential in mitochondria and lysosome

Mitochondrial membrane potential was evaluated using Rhodamine 123 (RH-123) fluorescent dye. RH-123 is a cationic dye, which electrophoretically accumulates into the mitochondrial matrix. However, 4-FPAC treated cells (Figure 9B) when stained with RH-123 showed less fluorescence compared to the control cells (Figure 9A) indicating that derivative treatment depolarized the mitochondrial membrane (Figure 9C). In a parallel study, the cells were stained with Acridine orange. AO being a weak base accumulates in lysosomes where it gets protonated and entrapped. However, when lysosomal membrane gets permeabilized, AO relocates itself into cytosol and gives green fluorescence. It has been observed that the cells treated (Figure 9D) with 4-FPAC emitted intense green fluorescence from the cytosol compared to control cells (Figure 9E). The results herein vividly exemplify that 4-FPAC at the given concentration disrupted the integrity of both mitochondria as well as lysosomal membranes presumably because of the increased oxidative stress as described previously²⁶.

4-FPAC affects genes regulating apoptotic pathway

Major genes of intrinsic and extrinsic pathways of apoptosis were analyzed in A549 cells treated with 4-FPAC. The results revealed that the expression levels of pro-apoptotic genes of intrinsic pathway like *BAD*, *BAX*, *cytochrome c*, *caspase 9*, *BID* etc. were upregulated in the treated cells compared to controls, nonetheless, *caspase 7* expression remained unaltered

(Figure 10A). In addition, the anti-apoptotic gene like *survivin* and *BCL2* were found significantly downregulated, along with the negative regulator of *p53* like *MDM2* and *β-catenin*, in the 4-FPAC treated cells (Figure 10B). Moreover, the study also revealed that compared to control cells, the transcript level expression of *AIF* and *PARP-1* remained low in the 4-FPAC treated cells (Figure 10B) which reaffirms that the 4-FPAC is not activating any pathway which can lead to necrosis.

Further, transcript level analysis revealed that genes of extrinsic pathway of apoptosis like *FADD*, *TRADD* and *caspase 8* were triggered by 4-FPAC treatment (Figure 10A). Thus, it can be construed that in 4-FPAC treated A549 cell line, both the mitochondria mediated intrinsic as well as the TRADD/FADD mediated extrinsic pathways are involved in inducing apoptosis wherein *BID* acts as a mediator between these two pathways and *caspase 3* acts as an effector caspase. The significant upregulation of caspase 3, at protein and transcript level, in the 4-FPAC treated cells (Figure 10C) further indicates that the derivative induced apoptosis by p53 mediated caspase dependent pathway.

Moreover, since 4-FPAC was found adversely affecting lysosomal as well as mitochondrial membrane integrity, it was thought necessary to study the involvement of these organelles in cell death and hence, the transcript levels of Cathepsin B a lysosomal protease, Calpain 2 a cysteine protease localized to the cytosol as well as mitochondria were checked. Results revealed that the expression of *calpain2* went down in the 4-FPAC treated cells whereas that of *cathepsin B* was significantly upregulated (Figure 10B) indicating the possibility of both lysosomal and mitochondrial mediated pathways in inducing apoptosis.

4-FPAC treatment reduces metastasis in A549 cell line

Cancer cell migration plays a decisive role in establishing metastasis and is a frequently used feature, to evaluate the anti-cancer property of any novel derivative. It initiates, with the remodeling of ECM components and is followed by migration to the distant niche. This remodeling is mostly governed by matrix metalloproteinases (MMPs) which degrade type-VI collagen, the main component of ECM²⁷. Here, we observed the effect of 4-FPAC on MMP-9 and MMP-2 the key players of invasion and metastasis of cancer. At transcript level there was significant decrease in *MMP9* and *MMP2* (Figure 11C). Similar decreasing trend of both the MMPs was noticed at protein (Figure 11A) and activity level (Figure 11B) too hence reaffirming the inhibitory role of 4-FPAC on matrix remodeling. Moreover, there was

upregulation in the expression of TIMP2 and TIMP4 (Figure 11C), the negative regulators of MMPs which further support the downregulation of MMPs thereby, minimizing the ECM degradation in the presence of derivative.

With remodeling of ECM, tumour cells start changing its typical phenotype for metastasis. First, cancer cell losses its anchorage dependency, cell-cell interaction and establishes rapid proliferation. These properties of cancer cell were evaluated by soft agar, aggregation and clonogenic assay. Soft agar assay was done for optimizing the anchorage independent growth of cell. Result showed that control cells (Figure 12C) had proliferated at normal rate on agar layer and formed larger colony. However, cells treated (Figure 12D) with 4-FPAC, when observed after 48h incubation, showed apparent reduction in the size of colony (Figure 12F). Nevertheless, no significant difference was observed in the number of colonies as compared to the control (Figure 12G). In order to reaffirm this outcome, clonogenic assay was performed, in which we observed that the derivative was negatively affecting the clonogenic property of cancer cell line (Figure 12E). Therefore, from both experiments it was confirmed that in presence of 4-FPAC the anchorage independent growth and proliferation capacity of cancer cell line was reduced. Nonetheless, a significant increase in aggregate size of cancer cells was observed when treated with IC_{50} concentration of 4-FPAC (Figure 13C). The average size of cell aggregate in case of control group was 60601 pixels (Figure 13A) but when treated with derivative, the mean size of aggregate was increased to 237339 pixels (Figure 13A), which showed that 4-FPAC increases the aggregation property of cancer cell and minimizes the metastasis property of cancer cell line *in vitro*.

At the molecular level, during metastasis of cancer cell, downregulation of E-cadherin, an epithelial cell surface adhesion molecule, upregulation of N-cadherin, a mesenchymal cell surface adhesion molecule and Vimentin, an intermediate filament protein were observed which are usually associated with epithelial to mesenchymal transition (EMT) which helps cancer cell to migrate from one niche to other²⁸. Therefore, we checked the expression of E-cadherin, N-cadherin and Vimentin at mRNA and protein levels. At transcript level there was significant decrease in N-cadherin however, increase in vimentin and E-cadherin was observed (Figure 14A). Whereas, at protein level, there was a minor increase in the expression of E-cadherin but decrease in vimentin and no significant change in N-cadherin was observed (Figure 14D). which illustrated that the derivative resists the morphological changes associated with EMT in A549 cells by increasing the epithelial property, under the

elevated levels of E-cadherin. It also minimizes the mesenchymal property of the cells by reducing vimentin. Downregulation of transcription factor Snail1, Snail2 and ZEB1 was observed in treated cell line (Figure 14C) which are known as repressor of E-cadherin²⁹. Further, effect of 4-FPAC on migration property of cancer cell line was estimated by *in vitro* wound healing assay. The result showed a significant reduction in percentage wound coverage in treated disc compared to control cells after 48h of treatment (Figure 15).

4-FPAC reduces angiogenesis in A549 cell line.

Angiogenesis is a major requirement for metastasis and many putative factors are known to influence the neovascularization in cancer tissue. Herein, we analyzed the transcript level expression of these factors and found that in 4-FPAC treated cells there was significant increase in *TGF-β*, *iNOS*, *VEGF-α*, *kdr* (Figure 14A, B). However, significant decrease was observed in *IL-8* and *IL-6*, whereas, there was no significant change was observed in the level of *IL-10* (Figure 14B). At protein level, TNF-α and iNOS were found upregulated whereas, IL-1β and IL-6 were downregulated and no significant change was observed in VEGF- α (Figure 14D).

4-FPAC reduces the expression of PI3K and Akt

PI3K is a major regulator of cell division³⁰, cell survival³¹, apoptosis³², EMT³³ and angiogenesis³⁴. There was no significant difference at the transcript level of *AKT* (Figure 16A) but in western blot analysis, treated cells were showing decrease in expression of both, AKT and PI3K with no significant change in Grb7 (Figure 16B), an upstream regulator of PI3K, which revealed that the derivative is affecting the pathway downstream of Grb7 at PI3K level.

4-FPAC make complex with p53 with 6 hydrogen and 2 pi-pi bonds.

Through *in silico* molecular docking, we showed that 4-FPAC docked efficiently with p53(5LGY) at the active site amino acid residue with docking score -5.89; Glide energy-48.38; Glide emodel (kJ/mol) score -67.9 and IFD score -420.03. ligand interacts with the protein target by 6 hydrogen and 2 pi- pi bonds, viz. Lys 132 (hydrogen bond with oxygen atom of ligand at a distance of 2.60 Å), Arg273 (hydrogen bond with oxygen atom of ligand at a distance of 2.13 Å), Arg 248 (form hydrogen bond with the NH atom of the ligand at a distance of 1.91 Å), Arg 280 NH group and Ala276 (NH interact with the 3-Oxo-butylaldehyde group of the ligand at a distance of 2.38 Å, 2.07 Å and 1.85 Å). 2H-Chromene

moiety of ligand forms pi-cation with Arg 273 (at a distance of 4.6 Å and 5.8 Å) (Figure 17).

HOMO- LUMO analysis in 4-FPAC

Highest occupied molecular orbital HOMO and LUMO energies were located on two distinct parts of 4-FPAC. The HOMO orbitals are located on 4-fluorobenzene ring and LUMO orbitals are located on the 3-acetyl coumarin ring; both distributed around the amine, oxygen, carbon and fluorine groups; indicating participation of these moieties during protein-ligand interactions. The calculated HOMO, LUMO and HOMO-LUMO energy gap for 4-FPAC were -0.2430eV, -0.1052eV and -0.1378eV respectively (Figure 18A)

Molecular electrostatic potential study of 4-FPAC

In general, the different values of the electrostatic potential are represented by different colors. It is accepted that the negative (red) and the positive (blue) potential regions in a mapped MESP represent regions susceptible to approach electrophiles and nucleophiles, respectively. The color code of these maps ranges between -192.2281 a.u (deepest red) and -23.1788 a.u. (deepest blue). Most positive electro potential coloured deepest blue (most electrophilic site), most negative electro potential coloured deepest red (most nucleophilic site)³⁶. In MESP map of 4-FPAC; the region having most negative potentials are over the oxygen and fluorine atom, and the region having most positive regions are over the hydrogen atom and the methyl group (Figure 18C).

Drug likeliness property of 4-FPAC

Drug likeliness properties such as molecular weight <500, clogP not greater than 5 with <5 hydrogen bond donors and >10 hydrogen bond acceptors satisfied the criteria for Lipinski's rule of five⁸. 4-FPAC has molecular weight of 355.3 hydrogen bond donor 1, hydrogen bond acceptor 7.5 satisfying the criteria of Lipinski's rule of five. The partial coefficient (QplogPo/w) and water solubility (QPlogS); crucial parameters for the estimation of absorption and distribution of drugs ranged between 2.329 and -4.519, respectively; cell permeability (QPPCaco); an important factor in regulating the drug metabolism and its transport across membranes, was 319.6 and the percentage of human oral absorption was found to be 85.41%.

DISCUSSION

Earlier, a string of coumarin derivatives were synthesized by adding different chemical substitution and their anticancer property was evaluated, based on which, 4-flourophénylacetamide-acetyl coumarin was chosen for further analysis as it showed lowest IC₅₀ concentration in A549 cell line⁷. In the present study, IC₅₀ concentration for NIH3T3, a non-cancerous mouse fibroblast cell line was estimated, which indicated that 4-FPAC had negligible toxicity towards normal cells, hence, it was further considered for comprehension of cytotoxicity, specificity towards cancer cells and effect on different aspects of metastasis in A549 cell line.

Initially, trypan blue assay was performed to understand the percentage cell death, which revealed that approximately 28% of cells were dead when challenged with IC₅₀ concentration of 4-FPAC. However, the reported metabolic viability in MTT assay was found to be 50% at this concentration, which highlights the quiescent stage of the cells, wherein they are not dead, but elicit arrested growth. Therefore, it could be deduced that 4-FPAC was not only showing cytotoxic but also cytostatic property. Further, flow cytometric analysis revealed that 4-FPAC arrests cell cycle at G₀/G₁ phase, which mostly occurs due to the presence of DNA damage³⁵. A concurrent comet assay confirmed the DNA damage in 4-FPAC treated cells. The DNA damage could be the reason behind the observed activation of p53 which leads to the activation of p21, a downstream target of p53 and a known inhibitor of CDK2, CDK4 and PCNA. When activated p21 binds to PCNA it inhibits the latter's activity³⁶ which was evident from the low protein level expression of PCNA in the 4-FPAC treated cells. In addition, inactivation of PCNA by p21 might prevent DNA repair and hence, induce cell cycle arrest at G₁ phase. Moreover, it has been reported that activated p21 inhibits G₁ phase progression by inhibiting CDK4-cyclin complex³⁷. Furthermore, it is documented that CDK2 when combines with cyclin E, the complex helps the cell to pass G₁ phase³⁸. In the present study the 4-FPAC treatment resulted in significant downregulation of CDK2 expression and hence, it was no longer available for CDK2-cyclinE complex formation, resulting in cell cycle arrest at G₀/G₁ phase and thereby inducing cell death in A549 cells.

It is well known that necrosis and apoptosis are the two major pathways which converge to cell death when treated with a cytotoxic compound. As necrosis is an uncontrolled process, it leads to sudden cell rupture, plasma membrane damage, ATP depletion and enhanced ROS

generation, which causes damage to neighboring cells as well. However, apoptosis characterized by cell rounding, membrane blebbing, and finally removal of cells through formation of apoptotic bodies, which would be engulfed by phagosome and further eliminated from the system without damaging neighboring cells³⁹. Herein, the mechanism of cell death was analyzed in 4-FPAC treated A549 cells by ETBr/AO staining, DAPI staining, LDH release assay and Comet assay. The microscopic analysis revealed apoptotic signs like cell rounding and membrane blebbing in the treated cells. Additional markers of apoptosis like chromatin condensation and DNA damage were also exhibited by the 4-FPAC treated cells as evident from the results of ETBr/AO, DAPI and Comet assay. Moreover, only basal level of LDH, a sign of necrosis, was found to be released from cells treated with IC₅₀ concentration of 4-FPAC. The above result therefore, indicates that 4-FPAC induces apoptosis in A549 cells at IC₅₀ concentration.

However, most of the known chemotherapeutic agents exert their cytotoxicity by elevating ROS beyond the threshold limit⁴⁰. Hence, intracellular ROS level was investigated by DCFH-DA assay and found that there was significant elevation in ROS concentration in cells treated with 4-FPAC. This elevated ROS may be responsible for apoptotic death observed in 4-FPAC treated A549 cells. As ROS is a common intracellular metabolite it regulates several cellular cascades, in cancer as well as in non-cancer cells, including cell survival, cell death, metastasis and angiogenesis⁴¹⁻⁴². Whenever, ROS is elevated by a pharmacological compound it induces apoptosis by disrupting mitochondrial membrane potential and ultimately damaging the mitochondrial membrane integrity that results in the release of *cytochrome c*, form apoptosome and ultimately activate caspase cascade⁴³. Moreover, it has been reported that Fas ligand (FasL) also elevate ROS and that signals the Fas associated death domain which further activate caspase 8 mediated apoptosis⁴⁴. Other than intrinsic and extrinsic pathway regulators, p53 a redox sensitive transcription factor is also involved in cell death, survival and DNA repair⁴⁵. It has been observed that ROS mediated DNA damage activates p53 mediated apoptosis in cancer cells⁴⁶. The present observations like loss of mitochondrial membrane potential, elevated levels of *FADD*, *cytochrome c*, *caspases 3* and *p53* confirm that ROS plays a pivotal role in the induction of apoptosis in 4-FPAC treated A549 cells.

Failure of antioxidant system leads to ROS induction that further stimulates p53 mediated apoptosis. Here, in this study a significant decrease in the activity of antioxidant enzyme

such as catalase and GPx was observed in A549 cells at 48h of treatment with 4-FPAC compared to that of control. Therefore, it can be deduced that reduction in the activities of these antioxidant enzymes might be the main contributor to the observed elevation of intracellular ROS in the treated cells.

As it is well known that elevated ROS is responsible for loss of mitochondrial as well lysosomal membrane potential, we investigated the mitochondrial membrane potential by Rhodamine 123 staining and lysosomal membrane potential by acridine orange methods and the results vividly shown that both of the organelles lost the membrane potential. Mitochondrial membrane permeabilization leads to release of *cytochrome c* and *AIF*, in which *cytochrome c* causes caspase dependent and *AIF* is responsible for caspase independent cell death⁴⁷ The transcript level analysis showed that *AIF* is downregulated and *cytochrome c* is upregulated in the 4-FPAC treated cells, hence it can be deduced that cell death in treated A549 is caspase dependent. The upregulated expression of *caspase 9*, *caspase 8*, and *cleaved caspase 3* in the treated cells further consolidate this notion. Moreover, Cirman et al. (2004) have opined that lysosomal membrane damage leads to release of Cathepsins, which subsequently activates Bid, Bax, Bad and releases cytochrome c from mitochondria. Additionally, it was reported that Bax directly affects lysosome when translocated from cytosol to lysosomal membrane⁴⁷. Therefore, mitochondrial membrane damage and lysosomal membrane damage act as positive feedback loop via Cathepsin induced Bid and mitochondrial released cytochrome c which were found to be upregulated in 4-FPAC treated A549 cells.

Furthermore, it has been documented that like ROS, iNOS too acts in a concentration dependent manner and differentially regulates various cellular functions⁴⁹. At low concentration iNOS acts as a signaling molecule and activates cell survival, proliferation, metastasis and angiogenesis whereas at high concentration it exerts anti-tumor activity⁵⁰. Moreover, the regulatory role of iNOS was reported in many types of cancers including brain tumor, melanoma and breast cancer⁵¹⁻⁵³. The dual role of iNOS is dependent on cell type, concentration of therapeutic and cellular environment. Chemo-preventive agents like 5-flourouracil and fenretinide are known to induce apoptosis in cancerous cells by activating iNOS⁵⁴⁻⁵⁵. The typical markers of iNOS mediated cytotoxicity are caspase dependent apoptosis, chromatin condensation, DNA fragmentation, p53 phosphorylation and cytochrome c release from mitochondria⁵⁶. Since, these markers were seen in 4-FPAC

treated cells, we can conclude that the observed hike in the level of iNOS has contributed its bit in inducing apoptosis in the treated A549 cells.

Parallely, the efficacy of 4-FPAC was tested for its potent anti-metastatic property. Metastasis is a complex process that involves multiple steps like rapid proliferation, EMT, invasion, cell migration and angiogenesis. When A549 cells were treated with 4-FPAC, significant reduction in the aggregation property, clonogenic capacity, and anchorage dependency for growth and migration was observed. In order to understand the molecular events involved behind these phenomena, specific markers of the pathways that facilitate various processes of metastasis, as highlighted above, were studied in 4-FPAC treated A549 cells at transcript and protein levels. Result revealed significant downregulation in the expression of Snail1, Snail2 and ZEB1 which are known transcription Factors to activate EMT⁵⁷ which leads to a morphological change in which cells acquire a mesenchymal type of morphology (increased vimentin and N-cadherin) and loses its epithelial characteristics like cell-cell adhesion molecules namely claudins and β -catenin⁵⁸ which was apparent in the result. Due to the loss of these adhesion molecules, cells become free to move away from organized structures. When A549 cells were treated with 4-FPAC noticeable reduction in clonogenic capacity of cells was observed which is further supported by downregulation of PCNA, a proliferation marker. In addition, reduction in the levels of adhesion molecules like claudin 3 and claudin 4 was also observed in the treated cells, which could be a function of Snail mediated expression of a transcriptional inhibitor named ZEB1. Similar observation by Lin and co-workers⁵⁹ give credence to the present result. It is reported that when p53 expression increases it degrades Snail2 via MDM2 interaction⁶⁰. Therefore, it is prudent to presume that the observed hike in *p53* expression might be the reason behind the reduction in *snail 2* level in the treated cells. Moreover, the compromised expression of *snail 2* in turn influence the expression of ZEB1, a downstream modulator of Snail pathway, resulting in substantial reduction of EMT in A549 cell challenged with 4-FPAC. Further study on other transcription factors are required to unlock the complete phenomenon of EMT. Therefore, it could be inferred that 4-FPAC affects the EMT initiation process by upregulating E-cadherin via Snail activated downregulation of ZEB1 in A549 cells.

However, once EMT has initiated, the process will be maintained by the autocrine loop of growth factors like TGF- β ⁶¹. The TGF- β chiefly support EMT by activating transcription factors like Twist, Snail1 and ZEB1 which downregulated E-cadherin, crucial for epithelial

characteristic, and upregulates Vimentin and N-cadherin⁶². TGF- β is also known to induce ROS by reducing the levels of antioxidant enzymes like Glutathione peroxidase, SOD and Catalase⁶³. It is also reported that tumor cells undergoing EMT secrete matrix metalloproteinases (MMPs) under the influence of Snail, which is activated by TGF- β and hypoxia⁶⁴. The MMPs further degrades the basement membrane and cells start migration from one site to other via lymph node. The activated Snail induces IL-8 and VEGF- α which initiates neo vascularization near tumor cells⁶⁵⁻⁶⁶. VEGF- α also activates EMT via HIF-1 α mediated Snail pathway⁶⁷. It was observed that 4-FPAC increases the expression of TGF- β which leads to the augmentation of ROS and thereby upregulating HIF-1 α . Nonetheless, this upregulation was not enough to prevent Snail degradation and release of MMP-2 and MMP-9, as both were found decreased in treated cells, at the same time decrease in protein level expression of IL-8 was also observed which might be because of downregulation of *snail* and MMPs as reported by Lewis et al.⁶⁷. Moreover, p53 is reported to be a negative regulator of VEGF- α promoter activity⁶⁹ and in the treated cells there was significant reduction in the expression of *p53* therefore, it can be inferred that p53 and Snail were the major inhibitors of angiogenesis in A549 cells treated with 4-FPAC.

Other factors have also been suggested to be involved in the initiation and maintenance of metastasis including IL-6, IL-10, TNF- α and IL-1 β which too were studied herein to corroborate the earlier described anti-metastatic property of 4-FPAC against A549 cells. IL-10 is reported to be a suppressor of metastasis and angiogenesis⁷⁰. However, in most of the lung cancer cases, of IL-6 remained upregulated to assist survival, proliferation, invasion, metastasis and EMT⁷¹⁻⁷². Most of the non-small cell lung cancer secrete IL-6 and TNF- α which promotes EMT, invasion and metastasis⁷³. IL-1 β , which is produced by cancer cell itself, acts on cancer cell by establishing a cross-talk with autocrine factors like MMPs, VEGF- α , IL-8, IL-6 and TNF- α hence, facilitate invasion and angiogenesis⁷⁴. In this study, significant elevation in the transcript levels of *IL-10* and a concomitant reduction in the mRNA levels of *IL-6* and *IL-1 β* in was observed in 4-FPAC treated A549 cells which reiterate the anti-metastatic potential of the compound in question. Nonetheless, the expression of TNF α was found significantly reduced in the cells subjected to 4-FPAC. However, apart from its reported prometastatic property, TNF- α is also an activator of Fas mediated apoptotic pathway and ROS mediated necrotic pathway⁷⁵ hence, its increase could be assisting the extrinsic pathway of apoptosis as describe previously.

Furthermore, attempt was also made to understand the effect of the 4-FPAC on PI3K/AKT pathway, one of the main mediators of cell survival, EMT, metastasis as well as angiogenesis and hence, a potential target for anticancer therapy. Recently it has been reported that one of the coumarin derivatives successfully hampered PI3K/AKT pathway in K562 cells⁷⁶⁻⁷⁷. Moreover, it is stated that upon activation PI3K phosphorylates AKT, a downstream target and positive regulator of the pathway, which subsequently phosphorylates and inactivates both BAX and BAD two proapoptotic proteins of intrinsic pathway of apoptosis⁷⁸. In addition, phosphorylated AKT is known to enhance the MDM2 expression and hence, counteracts the expression of p53⁷⁹. In the present study significant reduction in the transcript levels of AKT and MDM2 was observed in the A549 cells treated with 4-FPAC. Moreover, it was also noted that mRNA levels of BAD, BAX and p53 remained significantly high in the treated cells. Therefore, it is possible that exposure to 4-FPAC might have reduced the expression of AKT which resulted in the reduction of MDM2 level, leading to the activation of p53, BAD and BAX hence, induces apoptosis in A549 cells. Additionally, PI3K/AKT pathway is known to upregulate the potent inducers of EMT namely Snail, TWIST, MMPs and TGF- β ⁸⁰⁻⁸¹. Ablation of AKT pathway is also reported to inhibit nuclear accumulation of β -catenin and thereby EMT⁸⁴. The over expression AKT favors angiogenesis by increasing the expression of HIF-1 α ⁸². In this study we found that 4-FPAC downregulates the PI3K/AKT pathway thereby increasing apoptosis and concomitantly decreasing EMT, invasion and angiogenesis in A549 cell line.

Molecular docking is an automated computer algorithm which determines how a compound will bind the active site of the target macromolecule. Docking algorithm put the ligand in many different orientations in the active site of the target macromolecule and predict the pose with lowest energy and then computes a “score” for each pose. Score is based on their Van der Waals interactions, electrostatic interactions, solvation effects and entropic effects between ligand-target⁸⁶. Since target and protein both are flexible therefore it works as “hand and gloves” phenomenon where both adjust themselves to achieve the “best fit” orientation and confirmation and this overall phenomenon is called the induce fit⁸⁷. Molecular docking results indicates that the 4-FPAC interact strongly with p53 active site and inhibits the vital mechanism of cancer cell proliferation and metastasis.

The remarkable guideline to predict electronic property and reactivity of any compound is by frontier molecular orbital energies i.e. HOMO and LUMO where HOMO stands for

highest occupied molecular orbital which is correlated with the electron donating ability of the molecule. Whereas, LUMO stands for lowest unoccupied molecular orbital and correlated with electron accepting ability. HOMO and LUMO are used to narrate the electron density cloud around the molecule. High HOMO energy is predictive of high electrophilic attack whereas, high LUMO energy is predictive of high nucleophilic attack and Large HOMO-LUMO gap is related to high kinetic stability and low chemical reactivity and vice versa. In the same way, electrostatic potential is a physical property of a distribution of electric charge around the atom. A positive electric potential means that a positive charge will be repelled in that region of space⁸³. A negative electric potential means that a positive charge will be attracted. The HOMO-LUMO and MESP studies revealed that the derivative has very low HOMO-LUMO energy gap which make it highly reactive in nature.

Nearly 40% of drug candidates fail in clinical trials due to poor ADME (absorption, distribution, metabolism, and excretion) properties. These late-stage failures contribute significantly to the rapidly escalating cost of new drug development. The ability to detect problematic candidates early can dramatically reduce the amount of wasted time and resources, and streamline the overall development process. Therefore, incorporating ADME predictions as a part of the development process can generate lead compounds that are more likely to exhibit satisfactory ADME performances during clinical trials⁸⁴. 4-FPAC satisfy all the drug likeliness criteria also predicted to have a good bioavailability. These results of *in silico* studies substantiate the anticancer effects of the ligand 4-FPAC; consistent with our *in vitro* findings.

Overall, the present *in vitro* study vividly exemplified that the coumarin derivative 4-FPAC, at a dose of 0.16 nM, successfully hampered the proliferation, EMT, invasion, migration and angiogenesis in A549 cells. In particular, 4-FPAC exerts its effect through AKT mediated inhibition of p53 pathway. In brief, the derivative caused cell cycle arrest at G0/G1 by p53 induced p21 mediated inhibition of CDK2/CDK4-cyclin complex and induced apoptotic cell death by ROS evoked p53 mediated caspase dependent pathway which involves both mitochondrial and lysosomal compartments. Further, it was observed that 4-FPAC is effective curtailing metastasis and angiogenesis in A549 cells by p53 mediated downregulation of Snail, MMP-2,9 and IL-8. It is highly reactive in nature and satisfy the drug likeliness property and bioavailability. The currently observed antitumor and anti-angiogenic efficacy along with druggability of 4-FPAC on A549 cells suggests that it has

the potential to evolve as a promising novel chemotherapeutic agent against non-small cell lung cancer.

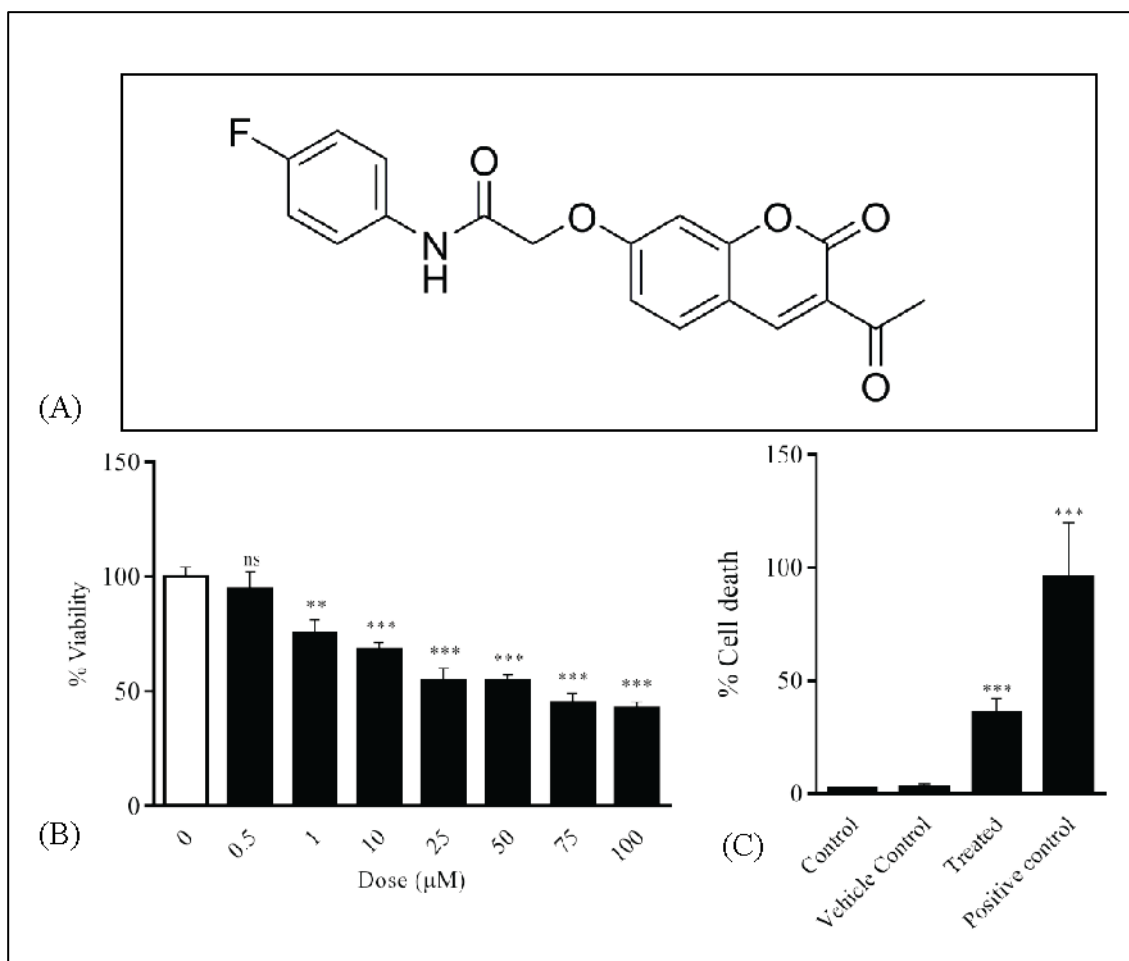


Figure 1: Structure of 4-FPAC and its cytotoxic effect:

(A) Chemical structure of derivative 4-FPAC; Cytotoxicity study (B) Cell viability assay for NIH3T3 cell line (C) Trypan blue dye exclusion assay in A549 cell line. *** $p \leq 0.001$, ** $p \leq 0.01$, ns-not significant.

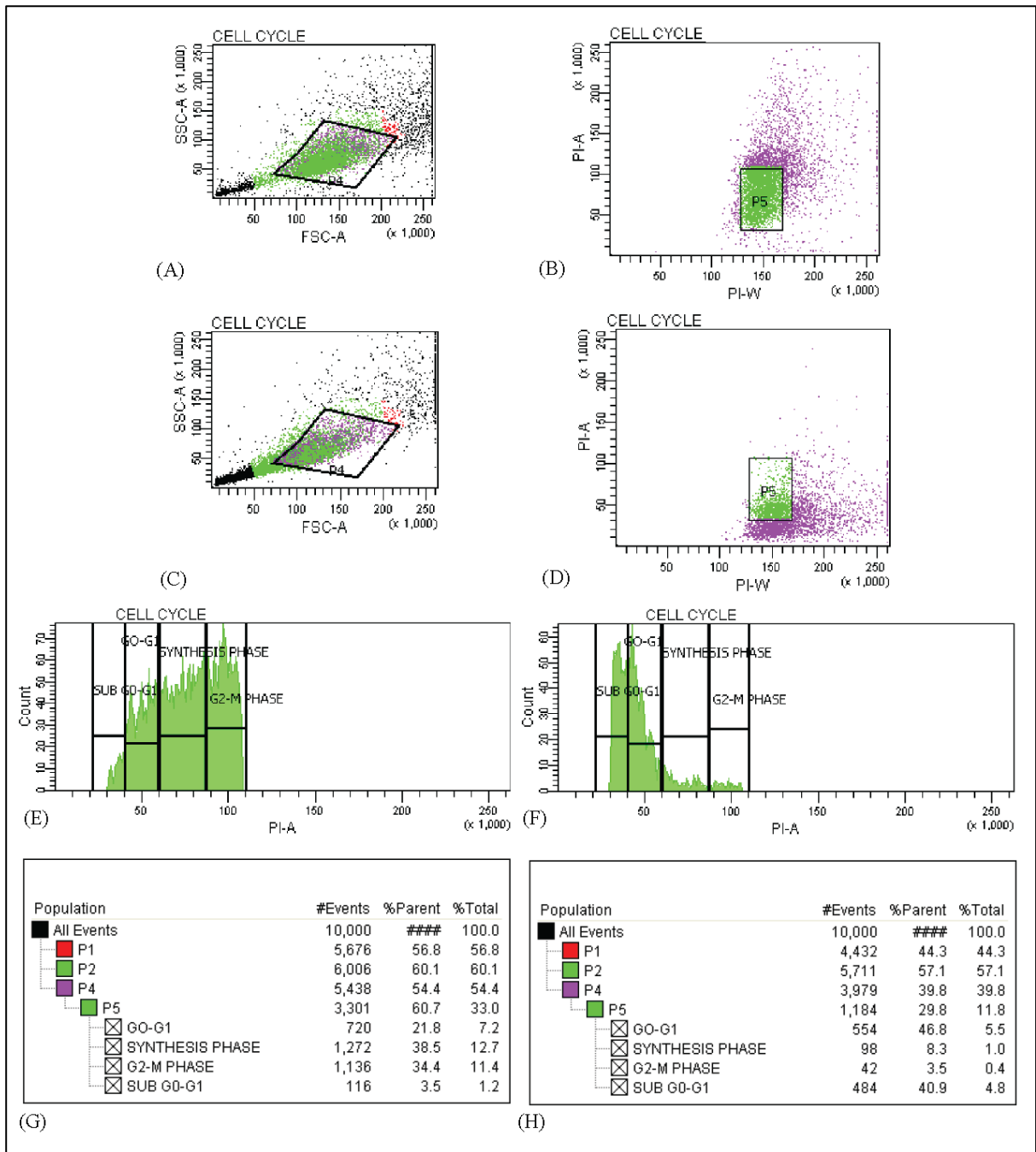


Figure 2: Flowcytometric analysis of cell cycle distribution in A549 cell line:

Histogram represents forward scatter (FSC-A) vs. side scatter (SSC-A) of control group (A) and treated group (C); Histogram represents pulse width (PI-W) vs. pulse area (PI-A) of control group (B) and treated group (D); Graph represents percentage of cell under various phases of cell cycle in control (E) and treated (F). Table represents number and percent of cell under various phases of cell cycle in control (G) and treated (H).

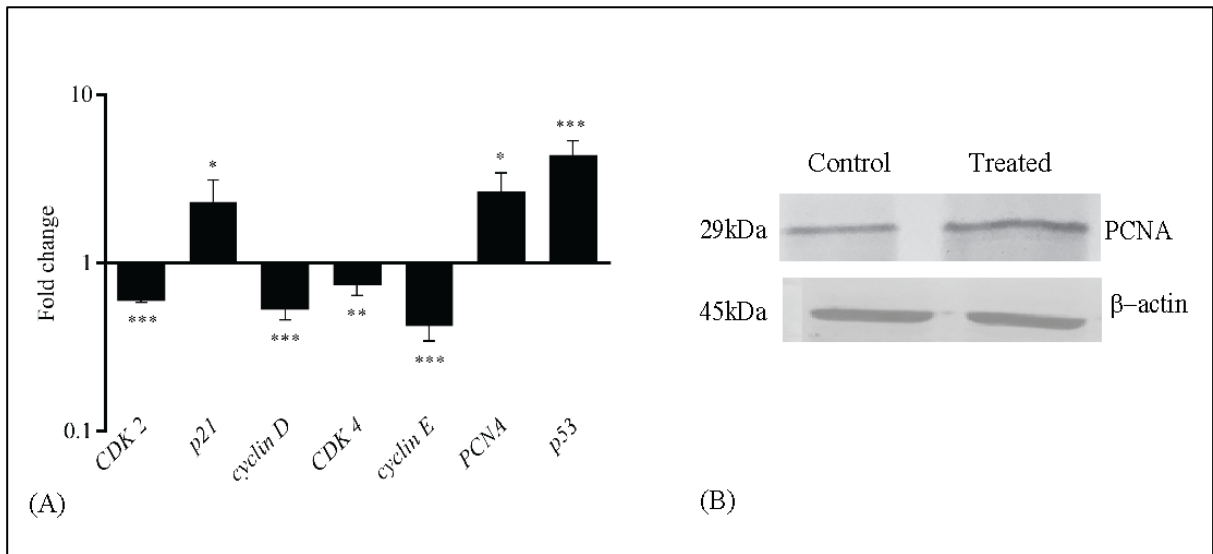


Figure 3: Effect of 4-FPAC on genes involved in Cell cycle regulation in A549 cell line:
 (A) Values are expressed as Mean \pm SEM. Fold change values for control is 1. *** $p \leq 0.001$, ** $p \leq 0.01$, * $p \leq 0.05$. (B) Western blot analysis of PCNA in control and treated group, β -actin was taken as internal control.

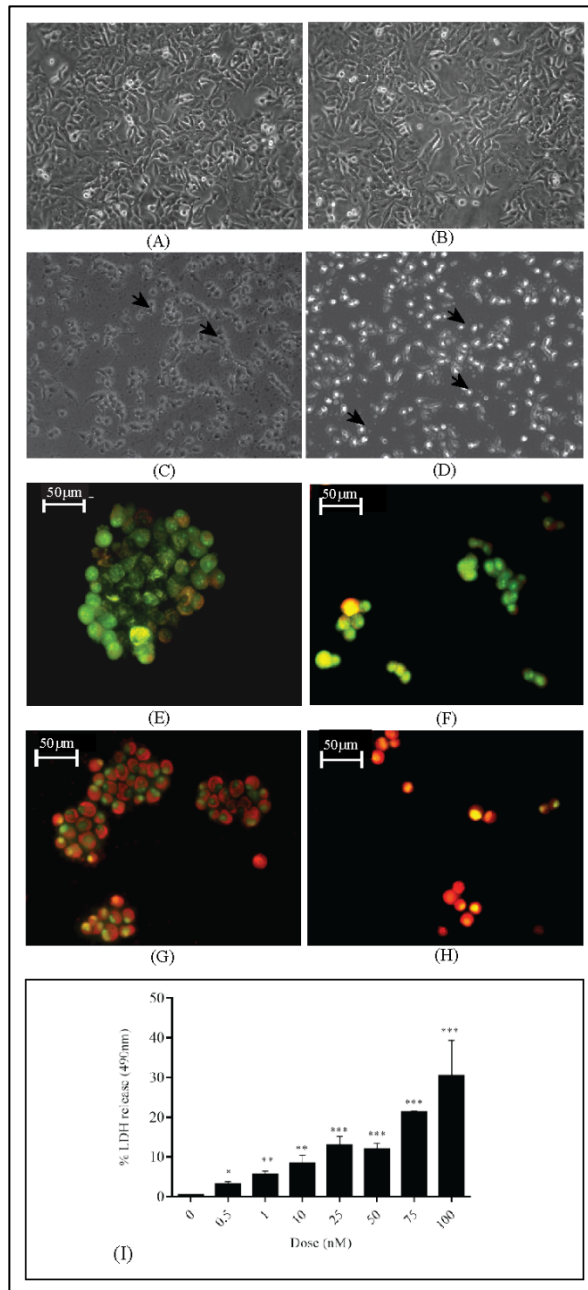


Figure 4. 4-FPAC cause apoptosis in A549 cell line. Cell Morphology study; (A) Control, (B) Vehicle Control, (C) Treated, (D) Positive control; Arrow indicates cell death. ETBr/AO staining for cell death study; (E) Control, (F) Vehicle control, (G) Treated, (H) Positive control. (C) LDH release assay; Graph represents Percentage LDH release under different concentrations (nM). Data are represented as mean \pm SD from three independent experiments. *** $P < 0.001$, ** $P < 0.01$, * $P < 0.1$.

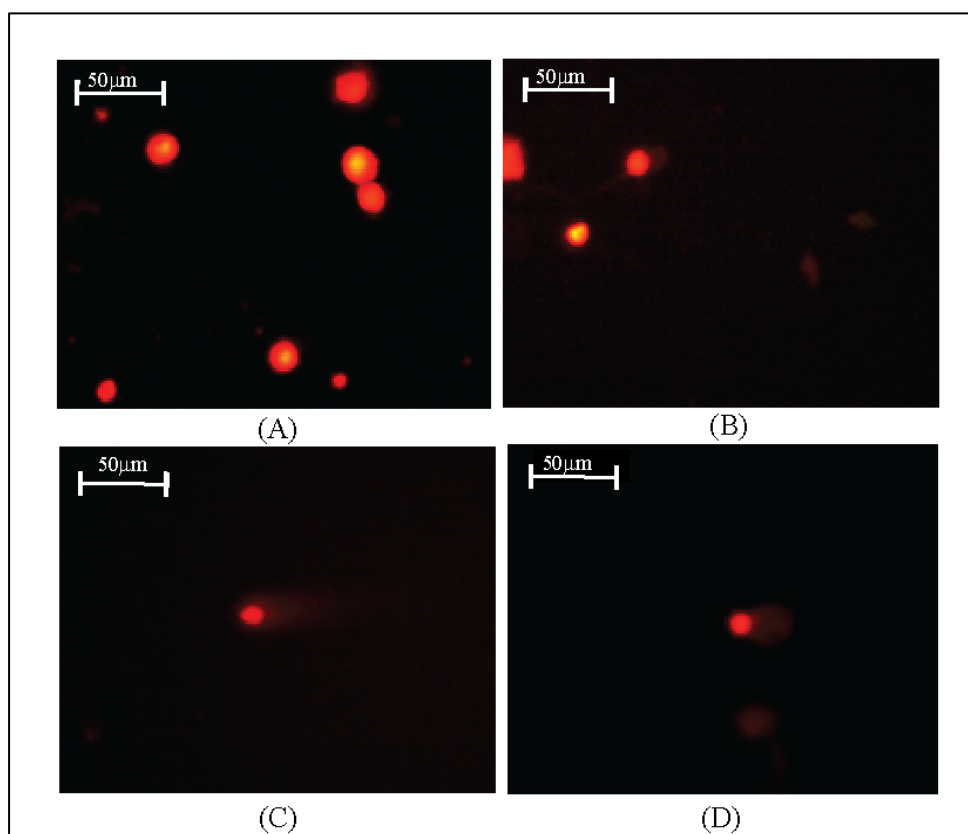


Figure 5. 4-FPAC shows genotoxicity towards A549 cell line. Comet assay for DNA damage; (A)Control, (B) Vehicle control, (C)Treated, (D) Positive control.

	Control	Vehicle Control	Treated	Positive control
Total comet length	98±5.09	112±11.09	204±12.67	186±4.43
Head length	93±4.19	105±12.05	139±12.37	133±1.891
Tail length	5±.034	7±0.901	65±9.05	53±1.891
% Head DNA	92.498±3.92	99.40±18.91	64.68.13±1.5	54.45±3.275
% tail DNA	7.5±.018	0.591±.003	35.31±2.85	45.53±2.677
Tail moment	0.37±.03	0.0413±.0001	58.26±0.33	24.31±1.334
Olive tail moment	0.3110±.03	2.367±.021	41.61±6.49	37.57±1.491

Table 1. Genotoxic effect of 4-FPAC on A549 cell line.

Comet assay result indicates DNA damage due to 4-FPAC. Data are represented as mean±SD, from three independent experiment.

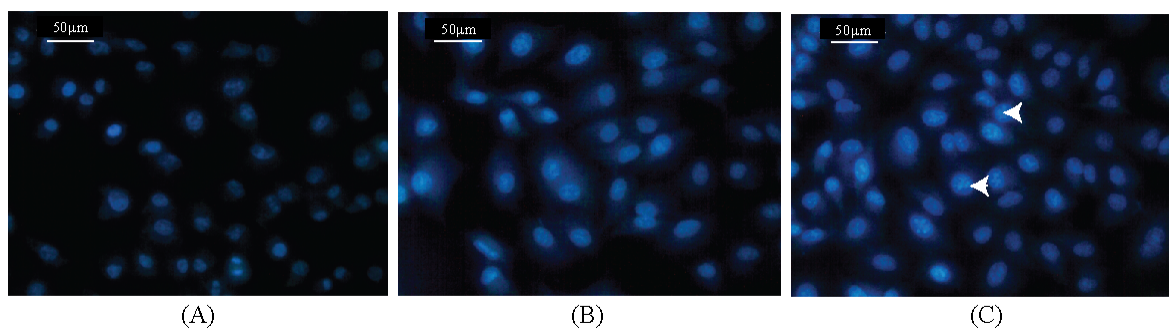


Figure 6. 4-FPAC shows genotoxicity towards A549 cell line. Nuclear staining with DAPI; (A)Control, (B)Vehicle control, (C)Treated. Arrow head indicates chromatin condensation.

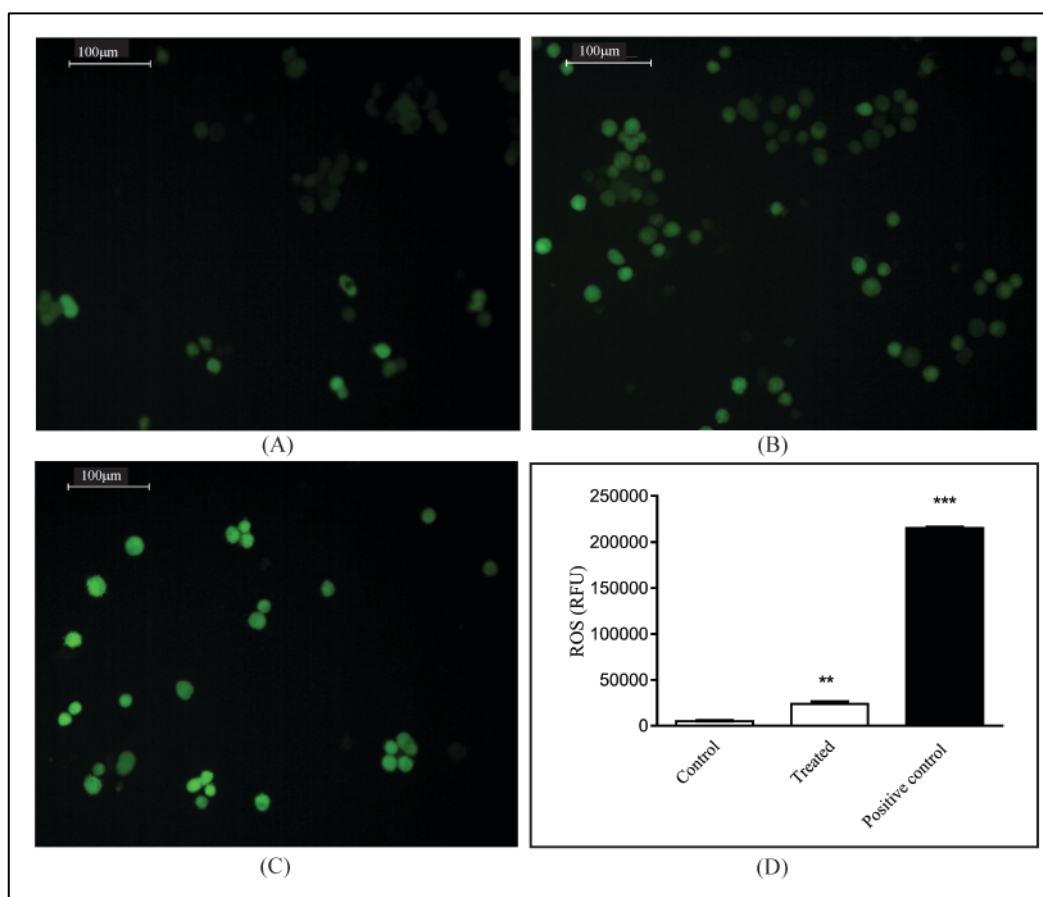


Figure 7. 4-FPAC increases Intracellular ROS concentration. Fluorescence microscopic images of A549 cell line, stained with DCFA-DH dye; (A) Control, (B) Treated and (C) Positive Control. (D) Analysis of ROS using fluorimeter; Graph represents relative fluorescence unit. Data are represented as mean±SD from three independent experiment. ***P<0.001, **P<0.01.

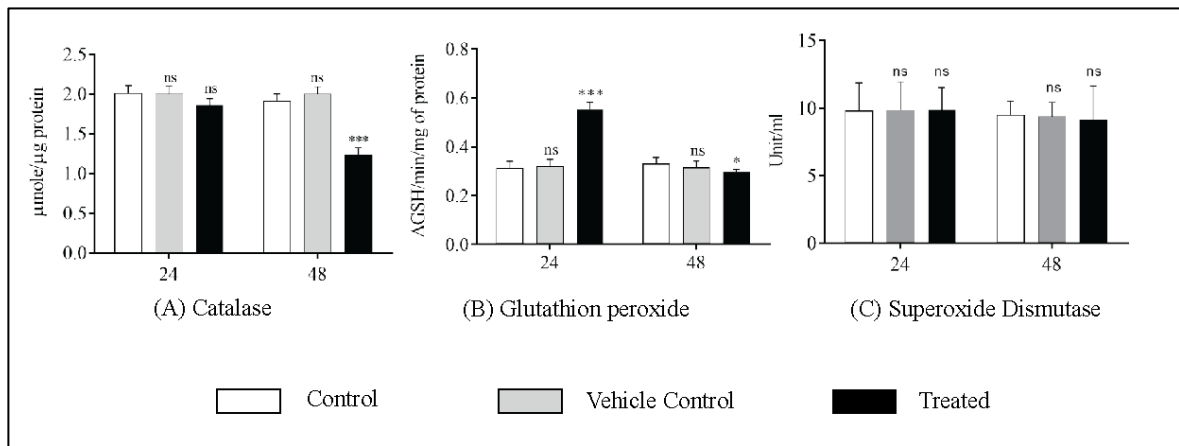


Figure 8. 4-FPAC affects Antioxidant enzymes in A549 cell line at 24h and 48h post treatment. (A) Catalase (B) Glutathion peroxidase (C) Superoxide dismutase. data are represented as mean±SD from three independent experiment and analyzed using an unpaired t-test, using GraphPad Prism software (GraphPad Software, San Diego, CA, USA). ***P<0.001, **P<0.01, ns; not significant.

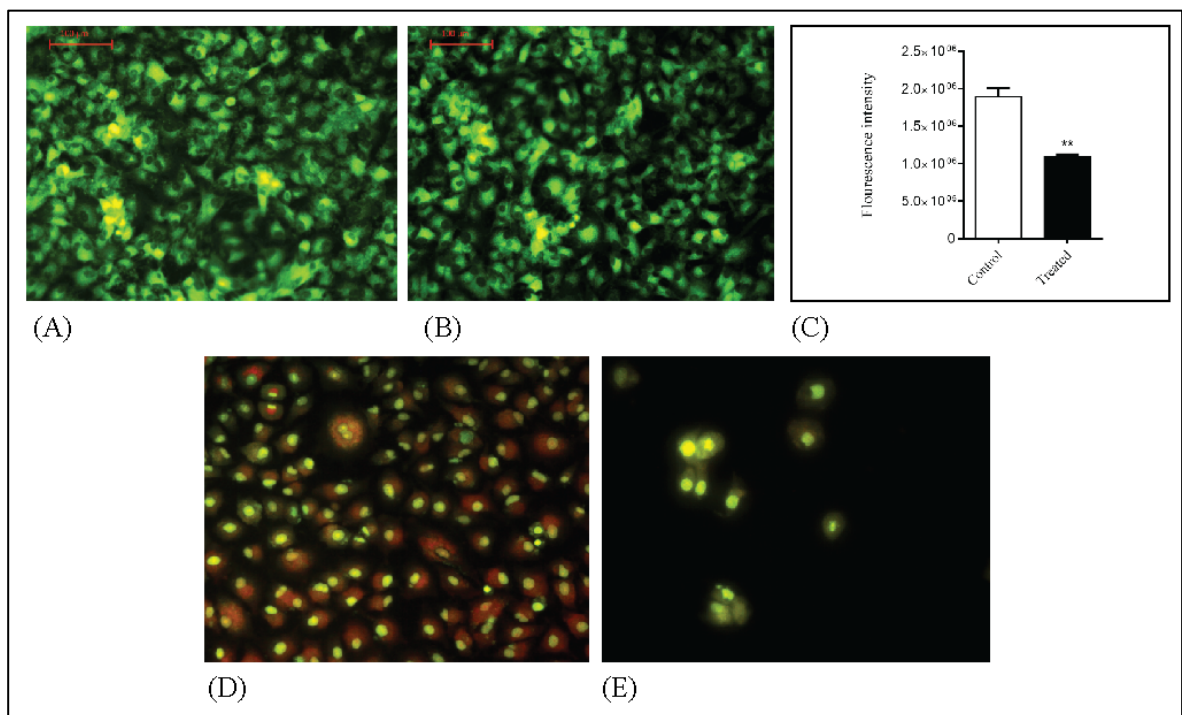


Figure 9. 4-FPAC affects Membrane potential in A549 cell line. Lysosomal membrane permeabilization (LMP); (A) Control and (B) Treated Mitochondrial membrane potential (MMP); (C)Control, (D)Treated. (E) Fluorescent intensity graph; control and treated cell line using Image J software (NIH). Data are represented as mean±SD, from three independent experiment. **P<0.01.

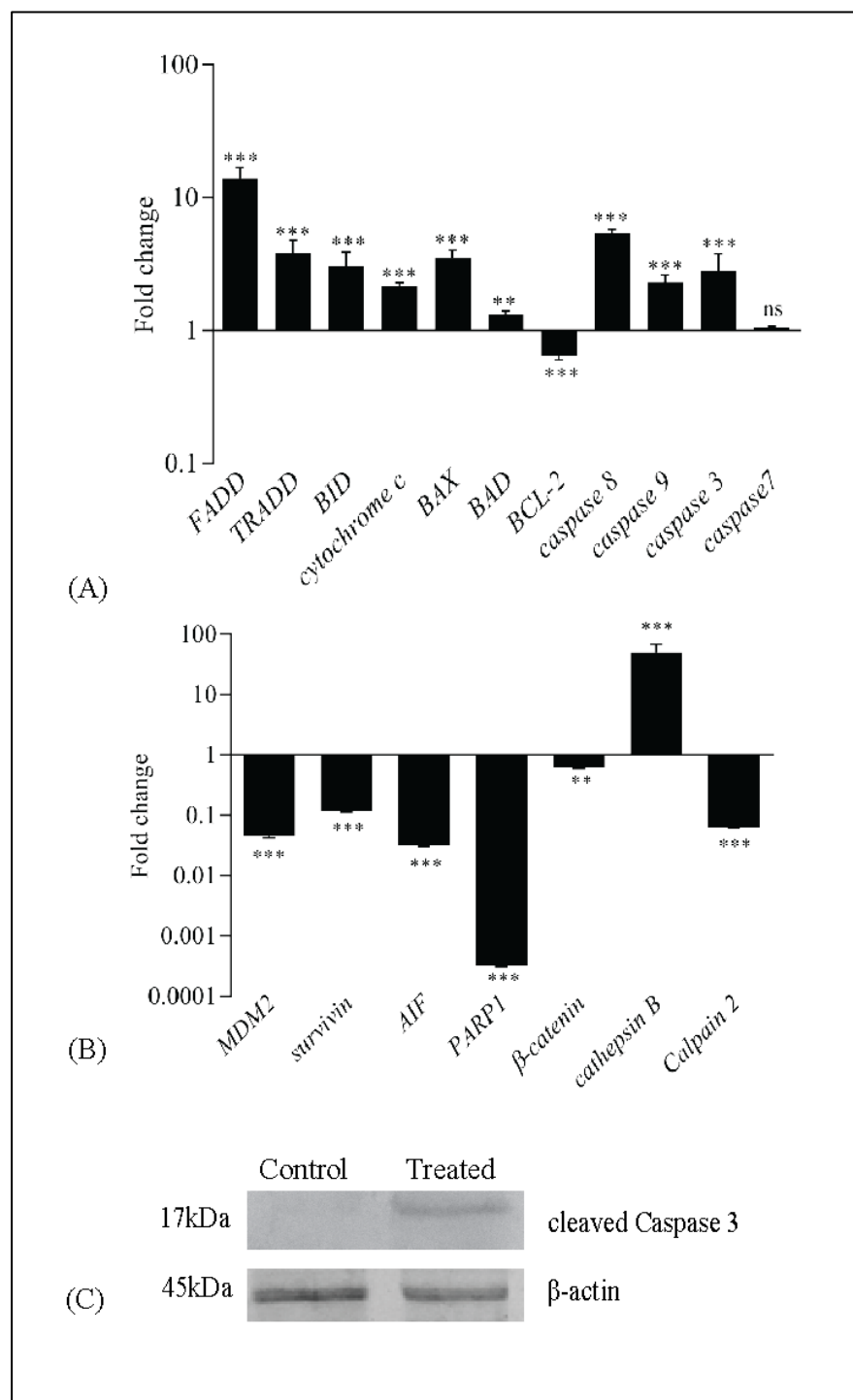


Figure 10. 4-FPAC regulates apoptosis at molecular level in A549 cell line. (A) and (B) qRT PCR study; Graph represent fold change of Treated mRNA vs. Control mRNA, expression level of control mRNA was assigned as 1.0. Experiment was performed in triplicate. Data were represented as mean \pm SD, ***P<0.001, **P<0.001, ns; not significant. (C) Western blot analysis of β -catenin and cleaved Caspase 3 in control and treated cell line.

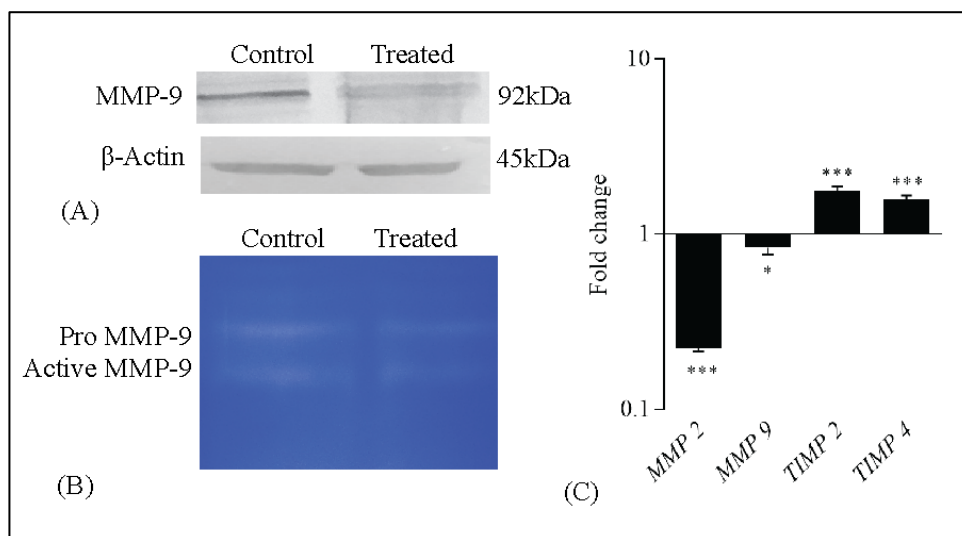


Figure 11. 4-FPAC reduces the MMP-9 expression in A549 cell line. (A) Western blot image of MMP-9 and β -actin. (B) Gelatin Zymography image of MMP-9; bands of pro and active MMP-9 in control and treated cell line. (C) Quantification of MMP-9 at transcription level by quantitative real time PCR; graph represents fold change of *MMP9*, *MMP2*, *TIMP2* and *TIMP4*. Expression level of control mRNA was assigned as 1.0. Experiment was performed in triplicate. Data are represented as Mean \pm SD, *** P <0.001, * P <0.1.

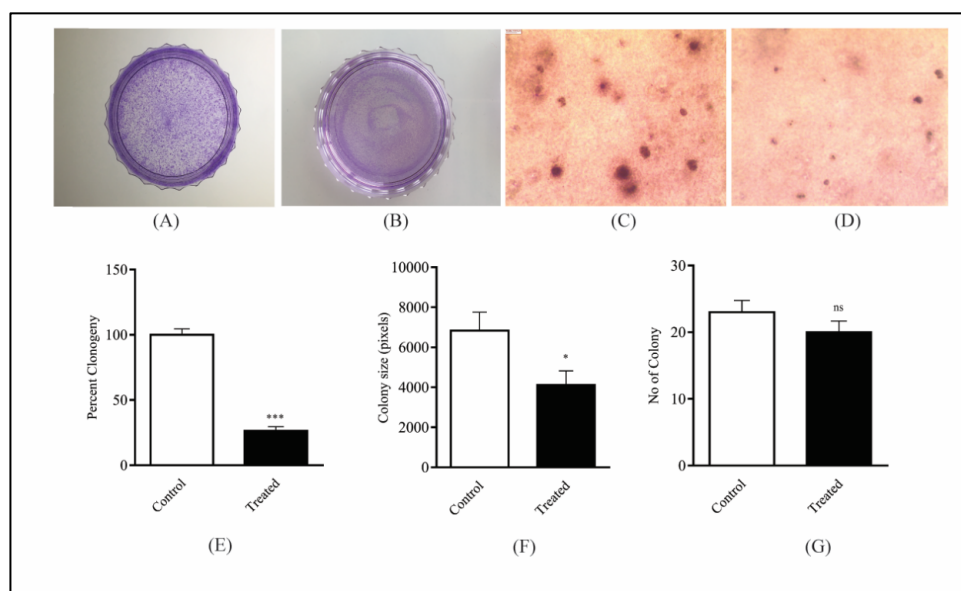


Figure 12. 4-FPAC reduces the anchorage independent growth and clonogenic property of A549 cell line. Clonogenic assay; Images of control(A) and treated(B) colonies at 48h post treatment. (E)Graph represents clonogenic inhibition in treated condition, experiment was performed five time in triplicate. Soft agar assay; images of colonies at 48h post treatment in control (C) and treated(D) cell lines, Graphs representing size of colony(F) and number of colony(G) on agar plate, experiment was performed in triplicate. Data are represented as mean \pm SD, * P <0.1, ns; not significant.

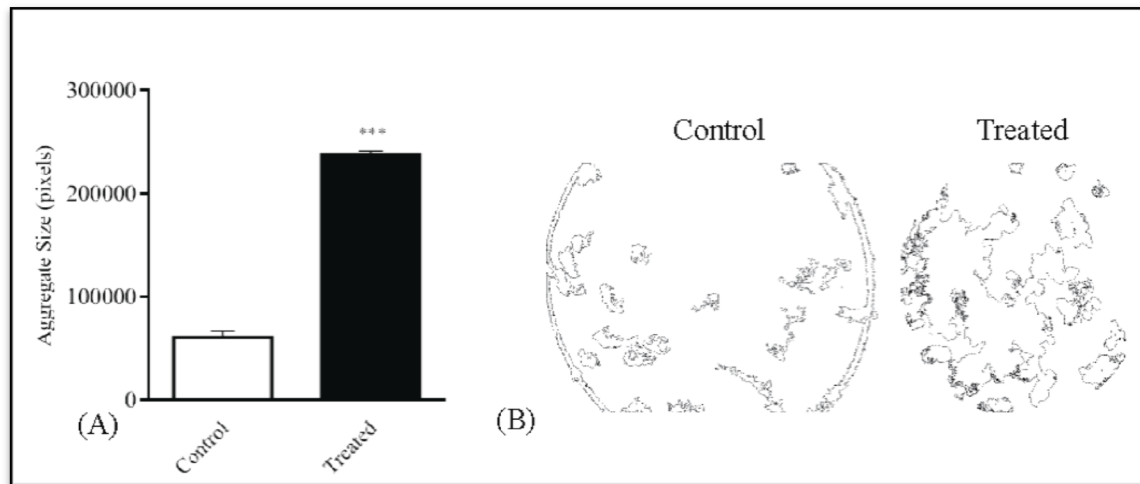


Figure13. 4-FPAC increases aggregate size in A549 cell line. Hanging drop assay; (A) Graph represents aggregate size (in pixels), estimated using Image J (NIH) software and plotted (pixels) using Graph pad prism 0.5. data are analyzed by Student's t-test. images of aggregate in control and treated cell at 0h and 48h. Experiment was performed in triplicate. Data are represented as mean \pm SD, ***P<0.001.

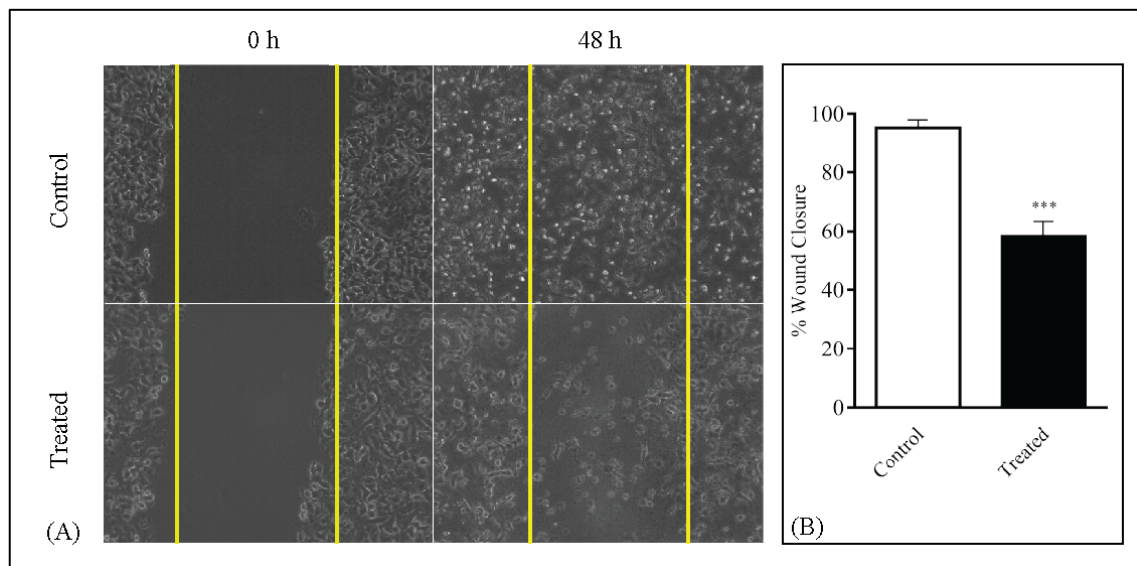


Figure 14. 4-FPAC reduces the migration property of A549 cell line. Wound healing Assay; (A)Optimization of cell migration in control and treated cell line at 0h and 48h post treatment. (B) Graph represents % wound area cover in control and treated cell line. Experiment was performed in triplicate. Data are represented as mean \pm SD, ***P<0.001.

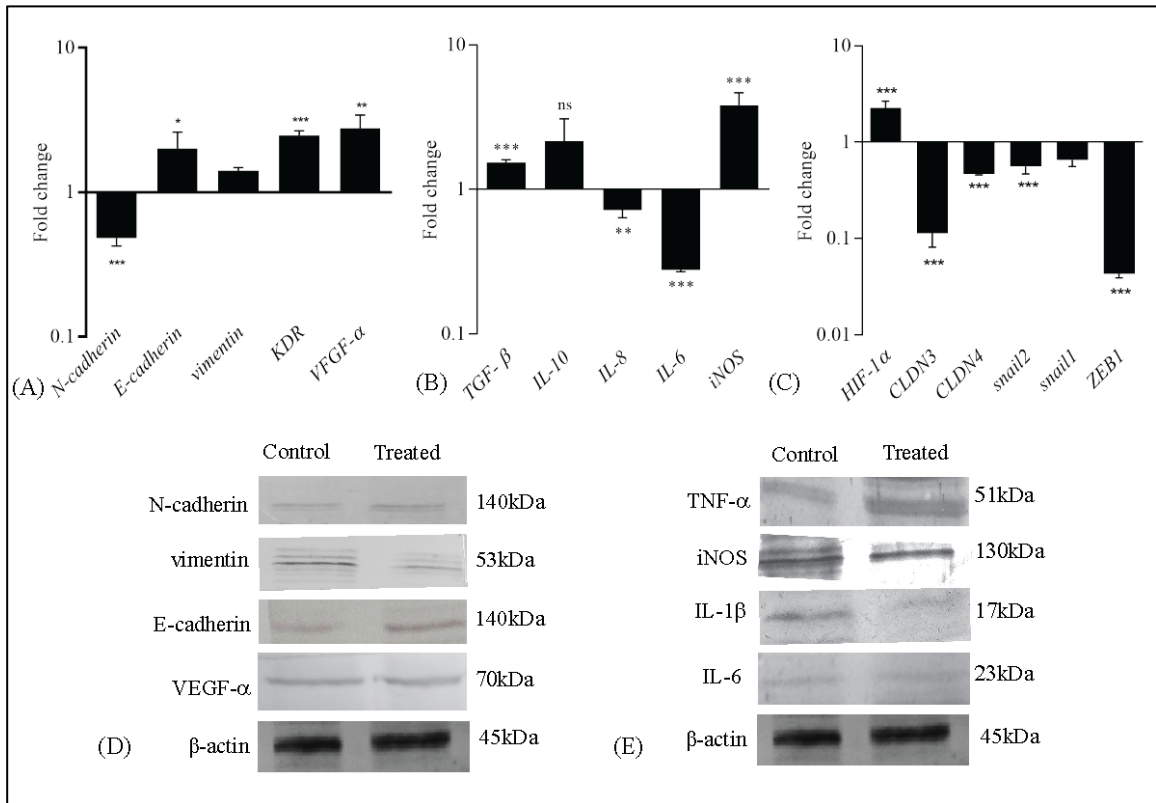


Figure 15. 4-FPAC reduces the Metastasis and angiogenesis by regulating expression of genes/proteins in A549 cell line. (A) Quantification of gene expression at transcription level by using qRT PCR; (A) (B) and (C) Graph represents fold change of genes regulating EMT, Angiogenesis and supportive cytokine, Expression level of control mRNA was assigned as 1.0. Experiment was performed in triplicate. Data are represented as Mean±SD, ***P<0.001, **P<0.01, *P<0.1, ns; not significant. Protein expression study; Western blot image of (D) N-cadherin, vimentin, E-cadherin, VEGF-α and β-actin (E) TNF-α, iNOS, IL-1β, IL-6 and β-actin in control and treated cell line.

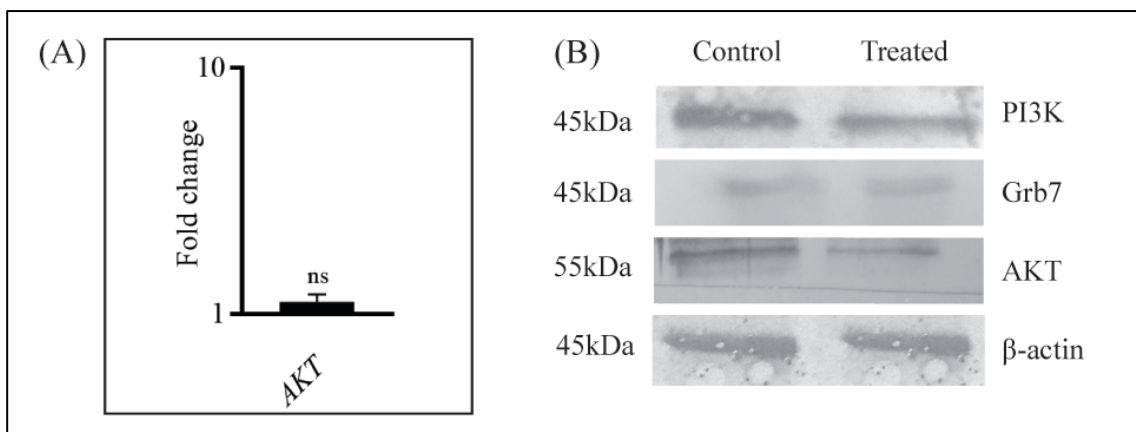


Figure 16. 4-FPAC affects PI3K/ AKT signaling pathway. (A) Quantification of AKT at transcription level by qRT PCR; Graph represents fold change of AKT. Expression level of control mRNA was assigned as 1.0. Experiment was performed in triplicate. Data are represented as Mean±SD, ns; not significant. (B) Western blot analysis of PI3K, AKT, Grb7 in control and treated cell line.

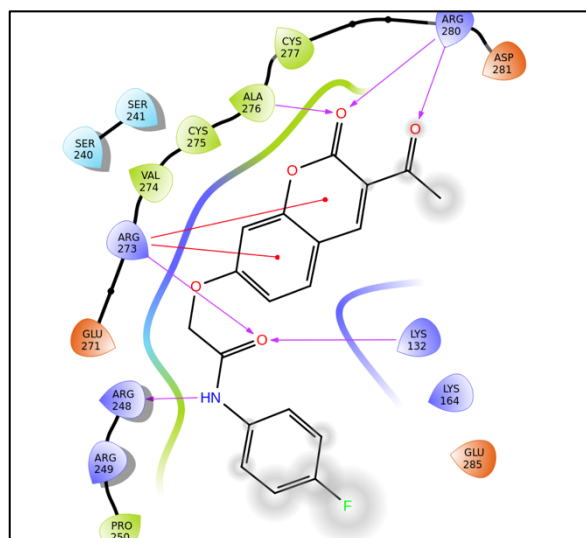


Figure 17. 2D docked pose of p53 (PDB ID; 5LGY) with 4-FPAC. Blue arrow indicates hydrogen bond and red indicates pi-pi interaction

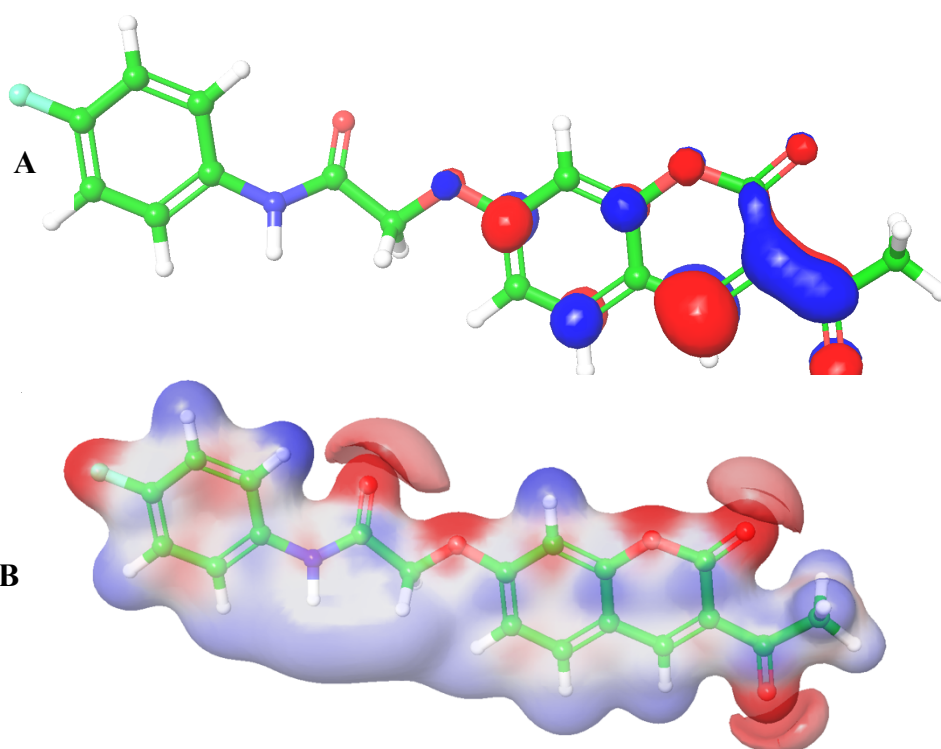


Figure 18. DFT analysis of 4 FPAC; (A) HOMO LUMO PLOT of 4-FPAC. (B) MESP map of 4-FPAC.

REFERENCES:

1. Thompson CB. Apoptosis in the pathogenesis and treatment of disease. *Science*, 1995;267(5203):1456-62.
2. Ferlay J, Soerjomataram I, Dikshit R, Eser S, Mathers C, Rebelo M, Parkin DM, Forman D, Bray F. Cancer incidence and mortality worldwide: sources, methods and major patterns in GLOBOCAN 2012. *International journal of cancer*, 2015;136(5):E359-86.
3. Finn GJ, Kenealy E, Creaven BS, Egan DA. In vitro cytotoxic potential and mechanism of action of selected coumarins, using human renal cell lines. *Cancer letter*, 2002; 183(1):61-8.
4. Hirsh J, Dalen JE, Anderson DR, Poller L, Bussey H, Ansell J, Deykin D. Oral anticoagulants: mechanism of action, clinical effectiveness, and optimal therapeutic range. *Chest*, 2001; 119(1):8S-21S.
5. Iwata N, Kainuma M, Kobayashi D, Kubota T, Sugawara N, Uchida A, Ozono S, Yamamuro Y, Furusyo N, Ueda K, Tahara E. The relation between hepatotoxicity and the total coumarin intake from traditional Japanese medicines containing cinnamon bark. *Frontiers in pharmacology*, 2016;7:174.
6. Egan D, O'kennedy R, Moran E, Cox D, Prosser E, Thornes RD. The pharmacology, metabolism, analysis, and applications of coumarin and coumarin-related compounds. *Drug metabolism reviews*, 1990; 22(5):503-29.
7. Durgapal SD, Soni R, Umar S, Suresh B, Soman SS. Anticancer Activity and DNA Binding Studies of Novel 3, 7-Disubstituted Benzopyrones. *Chemistry Select*, 2017; 2(1):147-53.
8. Lipinski CA. Lead-and drug-like compounds: the rule-of-five revolution. *Drug Discovery Today: Technologies*. 2004;1(4):337-41.
9. Chikara S, Lindsey K, Dhillon H, Mamidi S, Kittilson J, Christofidou-Solomidou M, Reindl KM. Enterolactone induces G1-phase cell cycle arrest in nonsmall cell lung cancer cells by downregulating cyclins and cyclin-dependent kinases. *Nutrition and cancer*, 2017; 69(4):652-62.
10. Olive PL, Banáth JP. The comet assay: a method to measure DNA damage in individual cells. *Nature protocols*, 2006; 1(1):23.
11. Pajaniradje S, Mohankumar K, Pamidimukkala R, Subramanian S, Rajagopalan R. Antiproliferative and apoptotic effects of *Sesbania grandiflora* leaves in human cancer cells. *BioMed research international*, 2014.
12. Maurya IK, Pathak S, Sharma M, Sanwal H, Chaudhary P, Tupe S, Deshpande M, Chauhan VS, Prasad R. Antifungal activity of novel synthetic peptides by accumulation of reactive oxygen species (ROS) and disruption of cell wall against *Candida albicans*. *Peptides*, 2011; 32(8):1732-40.
13. Paglia DE, Valentine WN. Hereditary glucosephosphate isomerase deficiency: A review. *American journal of clinical pathology*, 1974; 62(6):740-51.

14. Marklund S, Marklund G. Involvement of the superoxide anion radical in the autoxidation of pyrogallol and a convenient assay for superoxide dismutase. *European journal of biochemistry*, 1974; 47(3):469-74.
15. Sinha AK. Colorimetric assay of catalase. *Analytical biochemistry*, 1972; 47(2):389-94.
16. Chen QY, Shi JG, Yao QH, Jiao DM, Wang YY, Hu HZ, Wu YQ, Song J, Yan J, Wu LJ. Lysosomal membrane permeabilization is involved in curcumin-induced apoptosis of A549 lung carcinoma cells. *Molecular and cellular biochemistry*, 2012; 359(1-2):389-98.
17. Franken NA, Rodermond HM, Stap J, Haveman J, Van Bree C. Clonogenic assay of cells in vitro. *Nature protocols*, 2006; 1(5):2315.
18. Lui A, New J, Ogony J, Thomas S, Lewis-Wambi J. Everolimus downregulates estrogen receptor and induces autophagy in aromatase inhibitor-resistant breast cancer cells. *BMC cancer*, 2016; 16(1):487.
19. Yang L, Lee MM, Leung MM, Wong YH. Regulator of G protein signaling 20 enhances cancer cell aggregation, migration, invasion and adhesion. *Cellular signalling*, 2016; 28(11):1663-72.
20. Livak KJ, Schmittgen TD. Analysis of relative gene expression data using real-time quantitative PCR and the 2⁻ΔΔCT method. *Methods*, 2001; 25(4):402-8.
21. Vainer R, Cohen S, Shahar A, Zarivach R, Arbely E. Structural basis for p53 Lys120-cetylation-dependent DNA-binding mode. *Journal of molecular biology*, 2016; 428(15):3013-25.
22. Jayaraman A, Jamil K. Drug targets for cell cycle deregulators in leukemogenesis: in silico docking studies. *PLoS One*. 2014;9(1): e86310.
23. Bochevarov AD, Harder E, Hughes TF, Jeremy RG, Braden DA, Philip DM, Rinaldo D, Hall MD, Zhang J, Friesner RA. Jaguar: A high-performance quantum chemistry software program with strengths in life and material sciences. *Int J Quant Chem*. 2013;113:2110-42.
24. Khoshtabiat L, Mahdavi M, Dehghan G, Rashidi MR. Oxidative Stress-Induced Apoptosis in Chronic Myelogenous Leukemia K562 Cells by an Active Compound from the Dithio-Carbamate Family. *Asian Pacific journal of cancer prevention: APJCP*, 2016; 17(9):4267-73.
25. Ahmad KA, Iskandar KB, Hirpara JL, Clement MV, Pervaiz S. Hydrogen peroxide-mediated cytosolic acidification is a signal for mitochondrial translocation of Bax during drug-induced apoptosis of tumour cells. *Cancer research*, 2004; 64(21):7867-78.
26. Yang L, Zeng W, Li D, Zhou R. Inhibition of cell proliferation, migration and invasion by DNAAzyme targeting MMP-9 in A549 cells. *Oncology reports*, 2009; 22(1):121-6.
27. Wheelock MJ, Shintani Y, Maeda M, Fukumoto Y, Johnson KR. Cadherin switching. *J Cell Sci*, 2008; 121(6):727-35.
28. Peinado H, Olmeda D, Cano A: Snail, Zeb and bHLH factors in tumour progression. an alliance against the epithelial phenotype. *Nature reviews cancer*, 2007; 7(6):415.
29. Kumar A, Carrera AC. New functions for PI3K in the control of cell division. *Cell Cycle*, 2007; 6(14):1696-8.

30. Govindarajan M, Karabacak M, Suvitha A, Perandy S. FT-IR, FT-Raman, ab initio, HF and DFT studies, NBO, HOMO-LUMO and electronic structure calculations on 4-chloro-3 nitrofluorene. *Spectrochim Acta A Mol Biomol Spectrosc.* 2012; 89:137-48
31. Hsieh AC, Truitt ML, Ruggero D. Oncogenic AKTivation of translation as a therapeutic target. *British Journal of Cancer*, 2011; 105(3):329.
32. Parcellier A, Tintignac LA, Zhuravleva E, Hemmings BA. PKB and the mitochondria: AKTing on apoptosis. *Cellular signalling*, 2008; 20(1):21-30.
33. Xu W, Yang Z, Lu N. A new role for the PI3K/Akt signaling pathway in the epithelial-mesenchymal transition. *Cell adhesion & migration*, 2015; 9(4):317-24.
34. Jiang BH, Zheng JZ, Aoki M, Vogt PK. Phosphatidylinositol 3-kinase signaling mediates angiogenesis and expression of vascular endothelial growth factor in endothelial cells. *Proceedings of the National Academy of Sciences*, 2000; 97(4):1749-53.
35. Agarwal ML, Taylor WR, Chernov MV, Chernova OB, Stark GR. The p53 network. *Journal of Biological Chemistry*, 1998; 273(1):1-4.
36. Govindarajan M, Karabacak M, Suvitha A, Perandy S. FT-IR, FT-Raman, ab initio, HF and DFT studies, NBO, HOMO-LUMO and electronic structure calculations on 4-chloro-3 nitrofluorene. *Spectrochim Acta A Mol Biomol Spectrosc.* 2012; 89:137-4
37. Vermeulen K, Berneman ZN, Van Bockstaele DR. Cell cycle and apoptosis. *Cell proliferation*, 2003; 36(3):165-75.
38. Abbas T, Dutta A: p21 in cancer. intricate networks and multiple activities. *Nature Reviews Cancer*, 2009; 400-414.
39. Majno G, Joris I. Apoptosis, oncosis, and necrosis. An overview of cell death. *The American journal of pathology*, 1995; 146(1):3.
40. Trachootham D, Zhou Y, Zhang H, Demizu Y, Chen Z, Pelicano H, Chiao PJ, Achanta G, Arlinghaus RB, Liu J, Huang P. Selective killing of oncogenically transformed cells through a ROS-mediated mechanism by β -phenylethyl isothiocyanate. *Cancer cell*, 2006; 10(3):241-52.
41. Ushio-Fukai M, Nakamura Y. Reactive oxygen species and angiogenesis: NADPH oxidase as target for cancer therapy. *Cancer letters*, 2008; 266(1):37-52.
42. Trachootham D, Lu W, Ogasawara ma, Rivera-Del Valle Ni, Huang P. Comprehensive Invited Review. *Antioxidants & Redox Signaling*, 2008; 10(8).
43. Ozben T. Oxidative stress and apoptosis: impact on cancer therapy. *Journal of pharmaceutical sciences*, 2007; 96(9):2181-96.
44. Reinehr R, Becker S, Eberle A, Grether-Beck S, Häussinger D. Involvement of NADPH oxidase isoforms and Src family kinases in CD95-dependent hepatocyte apoptosis. *Journal of biological chemistry*, 2005; 280(29):27179-94.
45. Levine AJ, Hu W, Feng Z: The P53 pathway. what questions remain to be explored? *Cell death and differentiation*, 2006; 13(6):1027.
46. Ramsey MR, Sharpless NE. ROS as a tumour suppressor. *Nature cell biology*, 2006; 8(11):1213.

47. Lorenzo HK, Susin SA, Penninger J, Kroemer G. Apoptosis inducing factor (AIF): a phylogenetically old, caspase-independent effector of cell death. *Cell death and differentiation*, 1999 ;6(6):516.
48. Cirman T, Orešić K, Mazovec GD, Turk V, Reed JC, Myers RM, Salvesen GS, Turk B. Selective disruption of lysosomes in HeLa cells triggers apoptosis mediated by cleavage of Bid by multiple papain-like lysosomal cathepsins. *Journal of Biological Chemistry*, 2004; 279(5):3578-87.
49. Kågedal K, Johansson AC, Johansson U, Heimlich G, Roberg K, Wang NS, Jürgensmeier JM, Öllinger K. Lysosomal membrane permeabilization during apoptosis-involvement of Bax. *International journal of experimental pathology*, 2005; 86(5):309-21.
50. Lechner M, Lirk P, Rieder J. Inducible nitric oxide synthase (iNOS) in tumor biology: the two sides of the same coin. In *Seminars in cancer biology 2005*; Vol. 15, No. 4, pp. 277-289. Academic Press.
51. Zhang L, Liu J, Wang X, Li Z, Zhang X, Cao P, She X, Dai Q, Tang J, Liu Z. Upregulation of cytoskeleton protein and extracellular matrix protein induced by stromal-derived nitric oxide promotes lung cancer invasion and metastasis. *Current molecular medicine*, 2014; 14(6):762-71.
52. Cobbs CS, Brenman JE, Aldape KD, Bredt DS, Israel MA: Expression of nitric oxide synthase in human central nervous system tumors. *Cancer Research*, 1995; 55(4):727-30.
53. Loibl S, Buck A, Strank C, von Minckwitz G, Roller M, Sinn HP, Schini-Kerth V, Solbach C, Strebhardt K, Kaufmann M. The role of early expression of inducible nitric oxide synthase in human breast cancer. *European journal of cancer*, 2005; 41(2):265-71.
54. Ekmekcioglu S, Ellerhorst JA, Prieto VG, Johnson MM, Broemeling LD, Grimm EA. TumoriNOS predicts poor survival for stage III melanoma patients. *International journal of cancer*, 2006; 119(4):861-6.
55. Jiang J, Liu J, Zhu J, Yang C, Zhang A. Mechanism of apoptotic effects induced by 5-fluorouracil on human liver carcinoma Bel7402 cell line. *Chinese medical journal*, 2002; 115(7):968-71.
56. Simeone AM, Ekmekcioglu S, Broemeling LD, Grimm EA, Tari AM. A novel mechanism by which N-(4-hydroxyphenyl) retinamide inhibits breast cancer cell growth: the production of nitric oxide. *Molecular cancer therapeutics*, 2002; 1(12):1009-17.
57. Choi BM, Pae HO, Jang SI, Kim YM, Chung HT. Nitric oxide as a pro-apoptotic as well as anti-apoptotic modulator. *BMB reports*, 2002; 35(1):116-26.
58. Jiang J, Tang YL, Liang XH. EMT. a new vision of hypoxia promoting cancer progression. *Cancer biology & therapy*, 2011; 11(8):714-23.
59. Lin X, Shang X, Manorek G, Howell SB. Regulation of the epithelial-mesenchymal transition by claudin-3 and claudin-4. *PloS one*, 2013; 8(6):e67496.
60. Wang SP, Wang WL, Chang YL, Wu CT, Chao YC, Kao SH, Yuan A, Lin CW, Yang SC, Chan WK, Li KC. p53 controls cancer cell invasion by inducing the MDM2-mediated degradation of Slug. *Nature cell biology*, 2009; 11(6):694.

61. Xu J, Lamouille S, Derynck R. TGF- β -induced epithelial to mesenchymal transition. *Cell research*,2009; 19(2):156.
62. Vincent T, Neve EP, Johnson JR, Kukalev A, Rojo F, Albanell J, Pietras K, Virtanen I, Philipson L, Leopold PL, Crystal RG. A SNAIL1–SMAD3/4 transcriptional repressor complex promotes TGF- β mediated epithelial–mesenchymal transition. *Nature cell biology*,2009; 11(8):943.
63. Liu RM, Pravia KG. Oxidative stress and glutathione in TGF- β -mediated fibrogenesis. *Free Radical Biology and Medicine*, 2010; 48(1):1-5.
64. Ota I, Li XY, Hu Y, Weiss SJ. Induction of a MT1-MMP and MT2-MMP-dependent basement membrane transmigration program in cancer cells by Snail1. *Proceedings of the National Academy of Sciences*, 2009; 106(48):20318-23.
65. Hwang WL, Yang MH, Tsai ML, Lan HY, Su SH, Chang SC, Teng HW, Yang SH, Lan YT, Chiou SH, Wang HW. SNAIL regulates interleukin-8 expression, stem cell–like activity, and tumorigenicity of human colorectal carcinoma cells. *Gastroenterology*, 2011; 141(1):279-91.
66. Du R, Lu KV, Petritsch C, Liu P, Ganss R, Passegué E, Song H, VandenBerg S, Johnson RS, Werb Z, Bergers G. HIF1 α induces the recruitment of bone marrow-derived vascular modulatory cells to regulate tumor angiogenesis and invasion. *Cancer cell*, 2008; 13(3):206-20.
67. Mak P, Leav I, Pursell B, Bae D, Yang X, Taglienti CA, Gouvin LM, Sharma VM, Mercurio AM. ER β impedes prostate cancer EMT by destabilizing HIF-1 α and inhibiting VEGF-mediated snail nuclear localization: implications for Gleason grading. *Cancer cell*, 2010; 17(4):319-32.
68. Lewis AM, Varghese S, Xu H, Alexander HR. Interleukin-1 and cancer progression: the emerging role of interleukin-1 receptor antagonist as a novel therapeutic agent in cancer treatment. *Journal of translational medicine*, 2006; 4(1):48.
69. Mukhopadhyay D, Tsiokas L, Sukhatme VP. Wild-type p53 and v-Src exert opposing influences on human vascular endothelial growth factor gene expression. *Cancer research*, 1995; 55(24):6161-5.
70. Silvestre JS, Mallat Z, Duriez M, Tamarat R, Bureau MF, Scherman D, Duverger N, Branellec D, Tedgui A, Levy BI. Antiangiogenic effect of interleukin-10 in ischemia-induced angiogenesis in mice hindlimb. *Circulation research*, 2000; 87(6):448-52.
71. Shintani Y, Fujiwara A, Kimura T, Kawamura T, Funaki S, Minami M, Okumura M. IL-6 secreted from cancer-associated fibroblasts mediates chemoresistance in NSCLC by increasing epithelial-mesenchymal transition signaling. *Journal of Thoracic Oncology*, 2016; 11(9):1482-92.
72. Shang GS, Liu L, Qin YW. IL-6 and TNF- α promote metastasis of lung cancer by inducing epithelial-mesenchymal transition. *Oncology letters*, 2017; 13(6):4657-60.
73. Voronov E, Shouval DS, Krelin Y, Cagnano E, Benharroch D, Iwakura Y, Dinarello CA, Apte RN. IL-1 is required for tumor invasiveness and angiogenesis. *Proceedings of the National Academy of Sciences*, 2003; 100(5):2645-50.
74. Thorburn A. Death receptor-induced cell killing. *Cellular signalling*, 2004; 16(2):139-44.

75. Lin Y, Choksi S, Shen HM, Yang QF, Hur GM, Kim YS, Tran JH, Nedospasov SA, Liu ZG. Tumor necrosis factor-induced nonapoptotic cell death requires receptor-interacting protein-mediated cellular reactive oxygen species accumulation. *Journal of Biological Chemistry*, 2004; 279(11):10822-8.
76. Ma CC, Liu ZP. Design and synthesis of coumarin derivatives as novel PI3K inhibitors. *Anti-Cancer Agents in Medicinal Chemistry (Formerly Current Medicinal Chemistry-Anti-Cancer Agents)*, 2017; 17(3):395-403.
77. Simonyan L, Renault TT, da Costa Novais MJ, Sousa MJ, Côrte-Real M, Camougrand N, Gonzalez C, Manon S. Regulation of Bax/mitochondria interaction by AKT. *FEBS letters*, 2016; 590(1):13-21.
78. Abraham, Aswin G., and Eric O'Neill. PI3K/Akt-Mediated Regulation of p53 in Cancer. *Biochemical Society Transactions*, 2014; 42 (4): 798–803.
79. Hong KO, Kim JH, Hong JS, Yoon HJ, Lee JI, Hong SP, Hong SD. Inhibition of Akt activity induces the mesenchymal-to-epithelial reverting transition with restoring E-cadherin expression in KB and KOSCC-25B oral squamous cell carcinoma cells. *Journal of experimental & clinical cancer research*, 2009; 28(1):28.
80. Zuo JH, Zhu W, Li MY, Li XH, Yi H, Zeng GQ, Wan XX, He QY, Li JH, Qu JQ, Chen Y. Activation of EGFR promotes squamous carcinoma SCC10A cell migration and invasion via inducing EMT-like phenotype change and MMP-9-mediated degradation of E-cadherin. *Journal of cellular biochemistry*, 2011; 112(9):2508-17.
81. Fang, Dexing, David Hawke, Yanhua Zheng, Yan Xia, Jill Meisenhelder, Heinz Nika, Gordon B Mills, Ryuji Kobayashi, Tony Hunter, and Zhimin Lu: Phosphorylation of Beta-Catenin by Akt Promotes Beta-Catenin Transcriptional Activity. *The Journal of Biological Chemistry*: 2007; 282 (15), 11221–29.
82. Jiang BH, Jiang G, Zheng JZ, Lu Z, Hunter T, Vogt PK: Phosphatidylinositol 3-kinase signaling controls levels of hypoxia-inducible factor 1. *Cell Growth and Differentiation-Publication American Association for Cancer Research*, 2001; 12(7):363-70.
83. Gohlke H and Klebe G. Approaches to the description and prediction of the binding affinity of small-molecule ligands to macromolecular receptors. *Angewandte Chemie (International Edition in English)*, 2002; 2644–2676.
84. Hughes JP, Rees S, Kalindjian SB, Philpott KL. Principles of early drug discovery. *Br J Pharmacol*. 2001; 162(6):1239-49.

Candidate
(Ms. Shweta Umar)

Guiding Teacher
(Prof. B. Suresh)